Finite Element Modelling of FRCM-Confined RC Columns Exposed to Fire

FINITE ELEMENT MODELLING OF FRCM-CONFINED RC COLUMNS EXPOSED TO FIRE

by

Reem Talo

A Thesis presented to the faculty of the
American University of Sharjah
College of Engineering
In Partial Fulfilment
of the Requirements
for the Degree of

Master of Science in
Civil Engineering

Sharjah, United Arab Emirates

June 2023

Declaration of Authorship

I declare that this thesis is my own work and, to the best of my knowledge and belief, it does not contain material published or written by a third party, except where permission has been obtained and/or appropriately cited through full and accurate referencing.

Signed: Reem Talo

Date: 15/06/2023

Approvals

We, the undersigned, approve the Masters Thesis written by: Reem Talo

Thesis Title: Finite Element Modelling of FRCM-Confined RC Columns

Exposed to Fire

Date of Defense: 13/06/2023

Name, Title, and Affiliation	**Signature**
Dr. Farid Abed Professor Department of Civil Engineering Thesis Advisor	
Dr. Ahmed El Refai Professor Department of Civil and Water Engineering Laval University Thesis Co-advisor	
Dr. Rami Haweeleh Professor Department of Civil Engineering Thesis Examiner	
Dr. Basil Darras Professor Department of Mechanical Engineering Thesis Examiner	

Accepted by:

Dr. Fadi Aloul
Dean
College of Engineering

Dr. Mohamed El-Tarhuni
Vice Provost for Research and Graduate Studies Office of
Research and Graduate Studies

Acknowledgements

First and foremost, I would like to extend my deepest appreciation to my supervisors Dr. Farid Abed and Dr. Ahmed El Refai for their guidance, motivation, and assistance throughout the stages of this research. I would also like to extend my gratitude to the thesis committee members Dr. Rami Haweeleh and Dr. Basil Darras.

Special thanks to Engineers Arshi Faridi and Mohammad Ansari for their assistance in the laboratory work.

I would like to thank the American University of Sharjah and the Department of Civil Engineering specifically, for the financial support throughout the period of my degree completion.

Lastly, I would like to thank my family and friends for their support and motivation throughout this journey.

Abstract

Externally bonded fiber-reinforced polymers (FRP) have been widely used for strengthening and retrofitting applications. However, their efficacy is hindered by the poor resistance of epoxy resins to elevated temperature and their limited compatibility with concrete substrates. To address these limitations, fabric-reinforced cementitious matrix (FRCM), also known as textile reinforced mortar (TRM), systems have emerged as an alternative solution. This thesis presents the development of three-dimensional (3D) finite element (FE) models using ABAQUS software to investigate the performance of FRCM-confined RC columns exposed to fire. A parametric study was conducted to examine the behavior of confined columns under various conditions. The parameters studied include the concrete clear cover (40, 50, and 60 mm), the number of poly-paraphenylene benzobisoxazole (PBO) FRCM layers (0, 1, and 2 layers), the presence of a 30 mm thick insulation layer, and axial preloading. Numerical analysis revealed key findings. Increasing the concrete clear cover from 40 to 50 and 60 mm resulted in reductions of steel reinforcing bar temperatures by 14 and 27%, respectively, after 1 hour of fire exposure. Moreover, the inclusion of a 30 mm insulation layer reduced steel bar temperatures by 70% compared to uninsulated columns. Increasing the number of FRCM layers did not significantly affect load resistance duration, but increasing the preloading level significantly reduced the duration of load resistance. In addition to the numerical study, preliminary experimental tests were performed on PBO-FRCM confined cylinders subjected to different target temperatures (100, 400 and 800 °C) with different concrete strengths (30, 45, and 70 MPa) and number of FRCM layers (0,1, and 2). The experimental results highlighted the confinement effect of FRCM, particularly in cylinders with lower concrete compressive strength. Cylinders exposed to 100 °C exhibited a slight increase in strength, while no specific trend was observed in the variation of the compressive strength for cylinders heated to 400 °C. Specimens heated up to 800 °C experienced a significant reduction in strength, reaching up to 82%.

Keywords: Column, Finite element, Fire, FRCM, Reinforced Concrete, Strengthening

Contents

List of Figures

List of Tables

List of Abbreviations

FEA	Finite Element Analysis
FRP	Fibre Reinforced Polymer
FRCM	Fibre Reinforced Cementitious Matrix
PBO	Poly-paraphenylene Ben-zobisoxazole
RC	Reinforced Concrete
TRM	Textile Reinforced Mortar

Chapter 1. Introduction

1.1. Background

Fiber composite systems have been recognized as effective strengthening techniques for reinforced concrete (RC) members. Although concrete is the most used construction material given its many advantages including its high compressive resistance, high durability, and sufficient supply of raw materials, RC structures have been proven to deteriorate at some point in their lifetime and therefore, need to be strengthened. Retrofitting and/or strengthening of RC members is carried out for several reasons, including the need to resist higher levels of load than the design loads, degradation resulting from poor maintenance, corrosion of steel reinforcement, etc.

One of the most widely used strengthening techniques involves externally bonded composite materials, which enhance the mechanical properties of the concrete members including flexural, shear, and axial capacity. Fiber reinforced polymers (FRP) are one of the most common composite systems used and usually consist of unidirectional fibers embedded in a polymer adhesive matrix. They are highly efficient in strengthening applications due to their corrosion resistance, their large deformation capacity, their high strength-to-weight ratio, and their ease of installation.

Although FRP composites are generally efficient in strengthening applications, they have several drawbacks including the poor compatibility of their organic matrices with the concrete substrate. Moreover, the polymer matrices used in FRP have poor resistance to elevated temperatures, which is a serious concern in fire events. Organic resins lose their mechanical properties under high temperatures and release toxic fumes when temperature levels exceed their glass transition temperature (T_g), which is usually around 50-120°C [1].

To overcome the drawbacks linked to the organic matrices used in FRP, the fabric reinforced cementitious matrices (FRCM) strengthening systems, also known as textile reinforced mortars (TRM), were introduced. In these systems, open mesh textile fibers are embedded into inorganic mortar-based matrices, which are used as an alternative to the FRP organic matrices [2]–[9]. Figure 1 demonstrates the strengthening scheme for externally bonded FRP/FRCM in column confinement.

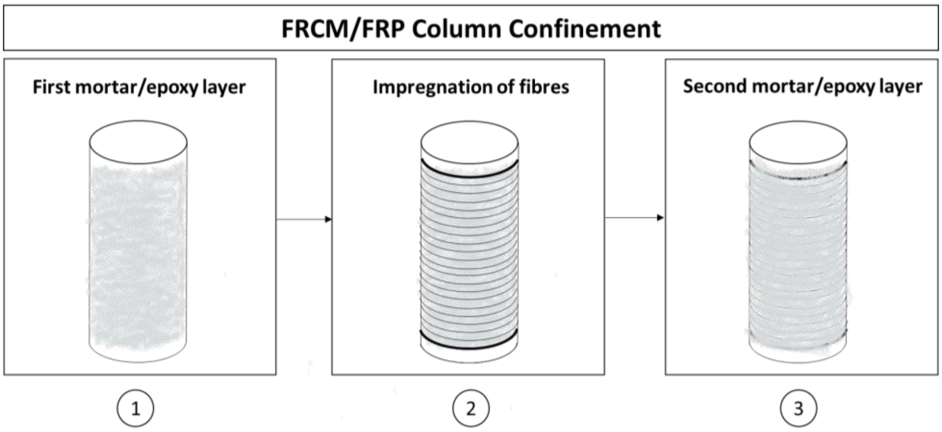

Figure 1: FRP/FRCM column strengthening scheme.

To evaluate the safety of structures during and after fire exposure, fire endurance should be assessed according to code requirements. Although the performance of fiber reinforced composite materials has been investigated in many studies at room temperature, their performance under high temperature exposure remains unclear and requires further research. There is limited evidence on the behaviour of FRP and FRCM under fire conditions, which requires full-scale fire tests that are usually costly and time consuming. Moreover, there are no specific standards and regulations to design and assess the fire resistance of fiber reinforced composites. One of the main concerns of structural fire engineers is to assure prevention of the structure's collapse during fire occurrence, at least until all occupants of a building have been given the chance to evacuate safely.

When RC columns are strengthened with circumferential FRP wrap, which increases the axial capacity through confinement, the loss of effectiveness of the FRP wrap due to the organic matrix is a serious concern [10]–[12]. According to ACI440.2R-08 [13], the strength of the FRP wrap is assumed to be completely lost in high temperature exposure conditions, unless it can be verified that the FRP temperature remains below its T_g. The use of FRCM systems instead of FRP wraps for column confinement could be a solution to achieve a better fire performance.

Several studies, including [14], [15] have proven the effectiveness of FRCM confinement at high temperatures. The objective of the proposed thesis is to evaluate the performance of FRCM-confined RC columns exposed to fire and to assess the feasibility of the FRCM confinement at high temperatures. Finite element models were developed using ABAQUS [16] and a parametric study was conducted considering four parameters: the concrete clear cover (40, 50, and 60 mm), the number of polybenzobisoxazole (PBO) FRCM layers (0, 1, and 2), the presence of a 30 mm thick insulation layer, and the applied axial load. The results are presented and discussed in the following sections.

1.2. Problem Statement

Although externally bonded FRCM systems are expected to have superior fire performance due to the inorganic binder, there is limited research in this area. Therefore, the feasibility of using the FRCM systems during and after high temperature exposure is questionable. On the other hand, FRP composites are significantly affected by elevated temperatures due to the epoxy-based resins used. This is one of the many drawbacks of the externally bonded FRP systems that has hindered their application in construction. The fire exposure significantly affects the mechanical properties of the binding matrix of FRP systems once heated above its glass transition temperature. If left uninsulated, FRP composites may burn since the organic resins are combustible, which can in turn lead to flame spread and release of toxic smokes [2]. Fires (including secondary fires) are extremely hazardous to buildings in terms of structural safety and threat to human lives; therefore, the assessment of FRCM performance at high temperatures is necessary given its potential improved fire resistance [12]. Although several studies have proven that FRCM composites provide adequate strength and performance at normal temperature [7]–[9], very limited studies have investigated their performance at elevated temperatures. Full-scale fire resistance tests used to assess the fire endurance of structural members can be very costly and time consuming. Therefore, numerical models are adopted as alternatives to study the performance of different structural members during fire conditions [17]. Rehabilitation of RC can also be a costly process, and the construction industry is constantly seeking efficient and sustainable strengthening and rehabilitation techniques as alternatives to conventional materials. Given the many advantages of FRCM systems over FRP systems, mainly attributed to the inorganic binding matrix, FRCM could be a promising alternative for retrofitting and strengthening applications, especially in terms of fire endurance.

1.3. Thesis Objectives

The primary aim of this study is to investigate the effect of fire on the performance of FRCM-strengthened RC circular columns. The objectives of this study can be summarized as follows:

- Develop finite element models to simulate the performance of FRCM-strengthened RC columns exposed to fire using ABAQUS [16].
- Evaluate the structural performance of the PBO-FRCM-confined RC columns during heat exposure and utilize the developed models to evaluate the feasibility of FRCM confinement for columns at high temperatures.
- Provide recommendations on the application of FRCM systems at high temperatures.

Chapter 2. Background and Literature Review

FRP and FRCM systems are widely recognized in strengthening and retrofitting applications under room temperature. However, their performance under high temperatures remains questionable and requires further research. This section discusses the performance of both systems in fire events along with the advantages and limitations of each system according to previous studies.

2.1. Fire Performance of FRP Systems

There has been increased interest in the utilization of FRP systems in several civil engineering applications over conventional materials due to their multiple advantages such as their resistance to corrosion, their high strength to weight ratio, and their ease of installation. FRP systems can be applied as externally bonded reinforcement as well as internal reinforcement as an alternative to steel bars. A common method for external FRP reinforcement is the use of bonded fiber sheets. FRP wraps used to confine RC columns are applied around the circumference of the column cross section to provide extra strength and ductility. Moreover, FRPs are used to improve the flexural and/or shear capacity by external bonding. They are also utilized to improve the flexural capacity of slabs. Nonetheless, one major drawback associated with FRP systems is the uncertainty linked to their performance at high temperatures, which has hindered their use in buildings and industrial structures [18]. FRP systems remain stable below the resin glass transition temperature; however, when this temperature level is reached, significant changes are observed. As temperature increases, the epoxy resin starts to decompose, and more changes occur in the properties of the composite material. Due to the physical and chemical processes that occur at elevated temperatures, the composite undergoes obvious strength and stiffness degradation [19].

An experimental study by Foster and Bisby [20] investigated the residual tensile strength of Carbon FRP (CFRP) and Glass FRP (GFRP) coupons after exposure to temperatures up to 400 °C considering two different resin systems. Specimens were exposed to the desired temperature for 3h, allowed to cool down to room temperature conditions, and then tested in direct tension. The results indicated a severe loss in the tensile strength (> 50%) when approaching the thermal decomposition temperature of the binding matrix (above 200 °C for both matrices). Moreover, the residual properties of FRP seem to be predominantly affected by the properties of the binding matrix. However, the type of fiber didn't appear to affect the residual performance.

Moreover, Hawileh et al. [21] studied the effect of temperatures up to 300 °C on the tensile strength and elastic modulus of CFRP, GFRP, and CGFRP (Hybrid) laminates. Specimens were subjected to a specified temperature for 45 min and left to cool down before being tested. According to the test results, the epoxy adhesives softened within the temperature range of 200-250 °C and burned at 300°C. The CGFRP laminates had better fire performance compared to the CFRP and GFRP sheets in terms of stiffness degradation. At 250°C, the elastic modulus of the CFRP, GFRP, and CGFRP laminates decreased by 28, 26, and 9% respectively, compared to the values obtained at room temperature.

To achieve satisfactory fire ratings for FRP-strengthened members, it is necessary to provide some sort of fire protection. An experimental study by Williams et al. [22] investigated the performance of insulated FRP-strengthened concrete slabs under fire exposure using four different insulation systems. The specimens were subjected to the ASTM E119 [23] standard fire temperature-time curve with no loads applied. The test results indicated that providing sufficient insulation thickness minimized the cracks and avoided the possibility of delamination of the protection layer as well as the concrete cover. Moreover, appropriately designed and sufficiently insulated FRP-strengthened RC members can display satisfactory fire performance; however, full scale tests in which the insulated FRP-strengthened slabs are subjected to load are required to confirm this observation.

2.2. Fire Performance of FRCM Systems

Over the past few decades, FRCM systems have been widely studied, as they constitute a promising alternative to FRP materials. There are limited experimental and analytical studies that have assessed their behaviour at high temperatures [6], [24].

Raoof and Bournas [25] examined the bond performance between TRM and FRP and the concrete interface under elevated temperatures. Double-lap direct shear tests were performed on specimens, which included two RC prisms connected by FRP or TRM layers on their opposite sides. The test parameters included the binding matrix (mortar and resin), the exposure temperature (up to 150 °C and 500 °C for FRP and TRM, respectively), the number of layers (3 and 4 layers), and the preloading condition (steady-state and transient). The test results revealed an overall excellent performance of TRM systems at elevated temperatures. Under steady state heating conditions, the TRM specimens were able to maintain an average of 85% of their bond strength at room temperature up to 400 °C. On the other hand, the FRP specimens were able to maintain only 17% of their bond strength at 150 °C. Under transient test conditions, the TRM specimens also outperformed the FRP ones in terms of both the time they maintained the applied load and the temperature reached before failure.

Donnini et al. [6] evaluated the mechanical performance of FRCM systems under high temperatures. C-FRCM was used in the experimental study including dry and organic resin coated fibers. The experimental study included uniaxial tensile and double shear tests performed at a temperature range between 20 and 120°C. The tensile specimens were exposed to temperatures of 80 and 120°C for a period of 100 min to ensure that the center of the failure zone had a temperature of about 90% of the oven temperature and directly tested. Shear test specimens were either tested directly after being exposed to 120°C for 100 min or after being exposed to the same temperature for one hour and allowed to cool to room temperature. According to the obtained results, the FRCM systems with dry (uncoated fibers) were able to maintain good bond to the substrate up to an exposure temperature of 120°C. However, the FRCM systems with coated fibers displayed a 70% reduction in their strength at 80°C in the tensile tests and 61% decrease in the peak load in the double shear tests. On the other hand, FRCM systems with coated fibers, which were cooled off to room temperature, experienced a decrease in the peak load of only 7% in the double shear tests, indicating good adhesion between the coating and the matrix after cooling.

Asgharigharakheili [26] investigated the performance of C-FRCM under high temperatures. The performance was evaluated in terms of tensile strength and stiffness degradation. The key parameters of the study were the number of layers (1, 2, and 3 layers), the fabric layer orientation (unidirectional and bidirectional), the heating condition (steady-state and transient), and the target temperature (ambient, 100°, 200°, 300°, and 400°C). Results of the steady-state tests revealed a significant decrease in the tensile strength of the tested specimens at elevated temperatures; however, the FRCM coupons retained about 50% of their tensile strength at temperatures as high as 300°C.

Only one-layer fabrics were tested under transient conditions with either 20 or 30 mm thickness. The thicker samples displayed improved insulation since the fabric grid required more time to reach the critical temperature leading to failure. For a 50% load level, the critical temperature increased from 300° to 375°C for the 20 and 30 mm thick samples, respectively.

2.3. Axial Strengthening

Salloum et al. [2] experimentally studied the effect of different elevated temperatures on the performance of circular RC columns strengthened with different techniques including CFRP confinement. Insulated and uninsulated CFRP-strengthened columns were subjected to temperatures up to 800°C for a period of 3h and loaded in axial compression until failure after cooling to room temperature. The increase in temperature from 100° to 400°C resulted in a decrease in the axial capacity of 9 and 28% for the uninsulated columns, respectively, with stiffness loss of 3 and 45%, respectively. Severe stiffness degradation at a temperature of 400°C was attributed to the epoxy surpassing its thermal decomposition temperature (about 345°C). On the other hand, insulated columns heated to a temperature of 500°C experienced a 13% decrease in their axial capacity, indicating the effectiveness of the insulation system. Insulated columns heated to a temperature of 800°C experienced 47% loss of their axial strength; however, the residual strength was 70% higher than that of their unstrengthened counterparts.

Chowdhury et al. [27] conducted full-scale fire tests on FRP-strengthened RC columns with and without supplemental fire protection. The results indicated that, although FRPs are sensitive to high temperatures, it was possible to achieve satisfactory fire endurance ratings for the FRP-strengthened columns by providing suitable fire protection. The insulated FRP-strengthened column was able to resist elevated temperatures for at least 90 min longer than the equivalent uninsulated FRP-strengthened column during testing. However, the insulation system was not able to maintain the temperature of the FRP system below its glass transition temperature.

Another study by Trapko [28] investigated the performance of CFRP- and C-FRCM-confined concrete cylinders under elevated temperatures. The specimens were exposed to temperatures of 40°, 60°, and 80°C over a period of 24 hours and directly tested until failure. According to the results, a 10% drop in the load-bearing capacity for every 20°C rise on average occurred for the CFRP-confined cylinders. However, the temperature increase had a slight impact on the capacity of the FRCM-confined cylinders, which dropped in the range of 5 to 10% from 40°C to 80°C, respectively.

Ombres [14] analysed the structural performance of thermally conditioned concrete cylinders confined with PBO-FRCM. The parameters of the study were the temperature used for the thermal conditioning, the fiber reinforcement ratio, and the concrete strength. Over a period of five days, the cylinders were exposed to constant temperature ranging between 20 and 250°C daily for four hours and cooled to room temperature. The specimens were then tested at room temperature until failure. According to the results, the load bearing capacity decreased with the elevated temperatures, yet the decrease was limited and was a result of the subsequent heating and cooling performed in the thermal conditioning stage. Although the results of the study clearly showed the effectiveness of the PBO-FRCM confinement at elevated temperatures, further experimental and analytical investigation are still needed.

A series of tests were conducted by Cerniauskas et al. [15] on CFRP- and TRM-confined concrete cylinders exposed to temperatures up to 400°C. The cylinders were kept at the target testing temperature for one hour prior to testing and then loaded concentrically until failure. The test results demonstrated that the efficiency of the FRP confinement decreased significantly with the increased temperatures, particularly after exceeding the glass transition temperature. On the other hand, the TRM confining system displayed superior performance compared to the FRP system at 400°C. Moreover, there was a minor loss of the strengthening action of the TRM wrapping system at temperatures between 100 and 200°C, probably due to the reduction in the compressive strength of the concrete at these temperature levels. However, the TRM-wrapped cylinders showed an unexpected enhancement in the strength at 400°C. The discrepancy in the tests results suggested that more tests should be conducted to fully understand the behaviour of the FRCM confinement under high temperatures.

2.4. Flexural Strengthening

Tan and Zhou [29] investigated the flexural performance of GFRP- and Basalt FRP (BFRP)-strengthened concrete beams with and without fire protection after exposure to elevated temperatures in an electrical furnace. The beam specimens were exposed to different target temperatures following the ASTM E119 [23] temperature-time curve and tested after cooling to room temperature. Elevated temperature led to a decrease in the initial stiffness, ultimate strength, and failure modes due to the deterioration of the material properties, which was more significant at higher elevated temperatures. The GFRP strengthening efficiency was reduced significantly in the temperature range of 500 to 700°C even with the presence of the fire-protection due to the thermal decomposition and volatilization of the matrix resin. On the other hand, the BFRP-strengthened beams displayed less deterioration in ultimate strength compared to the GFRP-strengthened specimens.

Bhatt et al. [30] conducted fire tests on insulated CFRP-strengthened T-beams and slabs subjected to combined thermal and structural load. Variables considered include the extent of strengthening (width of FRP sheet), the insulation thickness, and the applied load level. Results showed that the CFRP–concrete composite action was completely lost at a temperature much higher than the glass transition temperature of the polymer matrix. The deflection in the beams began to increase rapidly after the CFRP-concrete interfacial temperature exceeded 200 °C, which was significantly higher than the adhesive Tg (80°C). Therefore, neglecting the CFRP contribution to the strength and stiffness of a member under fire exposure leads to a conservative estimation of the fire resistance of the strengthened member. The test results showed that CFRP-strengthened beams and slabs can resist four and three hours of standard fire exposure, respectively, under service load conditions due to the protection of the fire insulation.

Another study by Ding et al. [31] experimentally evaluated the fire performance of Fiber-Reinforced inorganic Polymer (FRiP) systems compared to the FRP systems for beam strengthening and the behaviour of both composites was analysed before and after fire exposure. Results indicated that FRiP composites can significantly contribute to the strength enhancement of concrete beams. In addition, they displayed considerably improved resistance to fire relative to FRP. Although FRiP displayed inferior strengthening efficiency compared to FRP at room temperature, the FRiP composites could retain around 47% of their strengthening efficiency in ambient temperature conditions after fire exposure.

Raoof and Bournas [32] investigated the flexural behaviour of RC beams strengthened with TRM and FRP composites at ambient and elevated temperature. The studied parameters were the type of strengthening (TRM and FRP), the number of layers (1, 3, and 7), the type of textile material (Carbon, Glass, and Basalt), the surface condition of the textile (dry and coated), and the presence of end anchorages. Specimens were heated until the temperature between the adhesive and concrete substrate reached a temperature of 150 °C and then loaded until failure. TRM was more effective in strengthening the specimens at high temperature and maintained an average of 55% of its strength at ambient temperature. Moreover, increasing the number of layers enhanced the capacity of the specimens strengthened with TRM and affected the observed failure mode; however, increasing the number of layers did not influence the FRP-strengthened beams due to the premature failure of the adhesive matrix. TRM-strengthened specimens displayed different failure modes including fiber slippage, interlaminar shear, and debonding including parts of concrete cover whereas FRP-strengthened specimens only showed adhesive failure. Due to the identical adhesive failure observed for the FRP-strengthened beams, the type of textile did not have any effect. Moreover, coating the carbon textile with epoxy increased the effectiveness of the TRM specimen by 20% at elevated temperature. Providing end-anchorage had a significant impact on increasing the flexural capacity of the FRP-strengthened beams compared to the non-anchored ones; however, the anchorage effect on the TRM-strengthened beams was limited.

2.5. Shear Strengthening

Teta and Bournas [33] studied the performance of TRM and FRP in shear strengthening of rectangular and T-beams at ambient and elevated temperatures. The parameters investigated on the rectangular beams were the type of matrix for fiber impregnation (resin and mortar), the temperature of exposure (20°, 100°, 150°, and 250°C), the strengthening configuration (side, U, and fully-wrapped), the number of layers (2 and 3), and the textile properties (material and geometry). On the other hand, the effect of anchorage was investigated on the TRM-strengthened T-beams. All beams were heated until the target temperature was reached and then loaded while keeping the temperature constant. According to the obtained results, TRM was more effective in increasing the shear capacity of the beams compared to FRP at elevated temperature. The FRP effectiveness decreased drastically from 100° to 150°C; however, the TRM effectiveness was slightly affected when exposed to elevated temperatures. Moreover, the strengthening configuration had a significant effect on capacity enhancement for both TRM and FRP at high temperature. In particular, the fully-wrapped configuration was the most effective while the side bonded was the least effective.

2.6. Previous Finite Element Work

Kyaure and Abed [34] conducted a parametric study on corrosion damaged RC columns retrofitted with PBO FRCM. 3D finite element models were developed using ABAQUS[16] and validated against the experimental results conducted in a study by Tello et al. [9] on FRCM-strengthened RC circular columns. The investigated parameters in this study included the cross-section of the tested columns (square and circular), the number of FRCM layers (0, 1, 2, 3, and 4 layers), the pre-damage level (mild, moderate, and severe), the eccentricity ratio (0, 0.3, 0.5, 0.75, 1.0, 1.25, and 1.5), and the column length (short and slender). According to the obtained results, the PBO-FRCM system was able to restore and enhance the axial capacity and ductility of the columns. Moreover, there was a positive correlation between the number of confining layers and the axial capacity and ductility, which was more significant in circular columns.

A numerical study by Mahdy et al. [35] investigated the performance of FRP-strengthened and insulated RC columns subjected to fire using FE analysis. The proposed modelling approach consisted of two stages. The initial stage was a heat transfer analysis in which transient thermal load was applied according to the ASTM E119 [23] temperature-time curve. In the second stage, the obtained temperature data was used to perform a mechanical analysis. The proposed model was validated against standard fire results for several FRP confined and insulated RC columns from the published literature. The FE results agreed well with the experimental results in terms of temperature distribution and axial deformation response.

Dai et al. [36] developed 3D FE models using ABAQUS [16] to study the behaviour of insulated FRP-strengthened RC beams exposed to fire. The thermal and structural behaviour were considered through an initial heat transfer analysis followed by a structural analysis. To validate the accuracy of the proposed approach, temperature-time and load-deflection curves were compared to those of the experimental data. According to the FE results, the proposed model could predict the structural performance of insulated FRP-strengthened RC beams under standard fire exposure.

A numerical study by Mirzabagheri and Salem [37] evaluated the residual compressive strength of square RC columns after fire exposure. FE models were developed using ABAQUS [16] and a parametric study was conducted to study the effect of the applied load ratio (20 to 100%) and the column height (1, 500, 2000, 2500, and 3000 mm) on the residual axial capacity of the columns. The proposed modelling approach was verified against experimental results of a study by Nair and Salem [38], which evaluated the residual load-bearing capacity of square RC columns exposed to different standard fire exposure durations (1- and 2-h) while being subjected to different load ratios (20 and 40% of their design compressive strength). All the tested specimens were modelled and the obtained residual capacities agreed well with those of the performed experiments.

Roudari and Abu-Lebdeh [39]modelled several RC columns from an experimental test by Bikhiet et al[40] using ABAQUS [16]. The aim of the performed experiments was to obtain the residual axial capacity of square RC subjected to fire. The studied parameters included the concrete strength (300, 375, 425, and 500 kg/cm^2), the fire duration (0, 10, 15, and 20 min.), the applied load (10, 15, and 20 ton), the steel bar diameter, the reinforcement ratio (1.4, 2, and 3.6%), the cooling technique (room temperature or water jet), and the steel grade. Four columns were selected and modelled using ABAQUS[16] and the FE load-displacement curves were compared to those of the tests. There was close agreement between the FE and the experimental results and the proposed model predicted well the residual capacity of the square RC columns subjected to fire.

Chapter 3. Methodology

Fire simulation using ABAQUS software requires a 2-step modelling process in which the thermal and mechanical material properties are considered. This section discusses the modelling method that was used, the material properties that were input in ABAQUS, and the verification of the proposed model.

3.1. Finite Element Modeling

3.1.1. Materials

The material properties for concrete, steel, and FRCM systems used in the finite element simulation of FRCM-confined RC columns exposed to heat are discussed in the following sections.

3.1.1.1. Concrete

To study the behaviour of RC members under high temperature exposure, the thermal, mechanical, and deformation properties of concrete were considered in the model input. Like other materials, these properties change with the level of temperature associated with fire. The variation of these properties as a function of temperature allows the utilization of a mathematical approach to study the behaviour of RC members exposed to fire[17].

3.1.1.1.1. Thermal properties of concrete

The thermal properties of concrete should be accounted for in the finite element model to determine the heat distribution and obtain the nodal temperatures. The specific heat, the density, and the thermal conductivity, which control the temperature-dependent properties of concrete, were considered. At room temperature, the thermal conductivity of concrete ranges between 1.4 and 3.6 W/mK and decreases gradually with increase in temperature. This variation is mainly attributed to the change in moisture content as temperature levels increase. The specific heat of concrete ranges between 840 J/kgK and 1800 J/kgK at room temperature and is highly affected by the concrete moisture content[17]. The thermal conductivity, specific heat, and density relations with temperature were adopted for the concrete used in the FE model according to Eurocode 2[41].

3.1.1.1.2. *Mechanical and deformation properties of concrete*

In fire design, the primary mechanical properties that should be considered for concrete are the modulus of elasticity and the stress-strain response in both compression and tension. The modulus of elasticity of concrete significantly decreases with increase in temperature. This decrease is a result of the development of excessive thermal stresses and physical and chemical changes in the microstructure of concrete due to increase in temperature [17].

Figure 2 displays the compressive stress-strain curves that will be adopted for concrete in the modelled specimens according to Eurocode 2 [41]. The stress-strain relationship of concrete in compression is generally characterized by a linear response at the beginning, followed by a parabolic response until ultimate compressive strength is reached, and finally a descending branch. The compressive strength of concrete decreases with increase in temperature, unlike its ductility, which increases at higher temperature levels. This phenomenon leads to a decrease in the slope of the stress-strain curve with increase in temperature. Elevated temperature has a significant impact on the compressive stress-strain behaviour of concrete, particularly above 500°C. As temperature increases, the strain corresponding to the peak stress can reach up to four times the strain at room temperature [17]. The ABAQUS [16] Concrete Damage Plasticity model was adopted to integrate the nonlinear behaviour of concrete in compression and tension versus the temperature exposure [34].

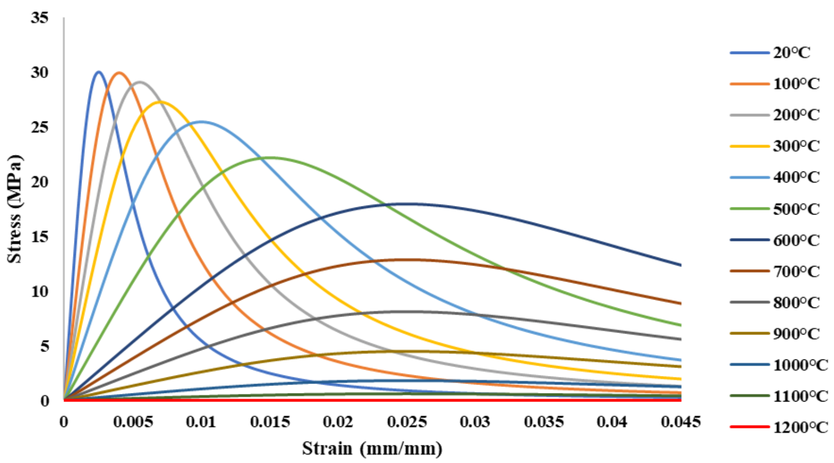

Figure 2: Concrete compressive stress-strain curves [41].

The tensile stress-strain curves were adopted for concrete according to Eurocode 2 and are shown in Figure 3 [41].

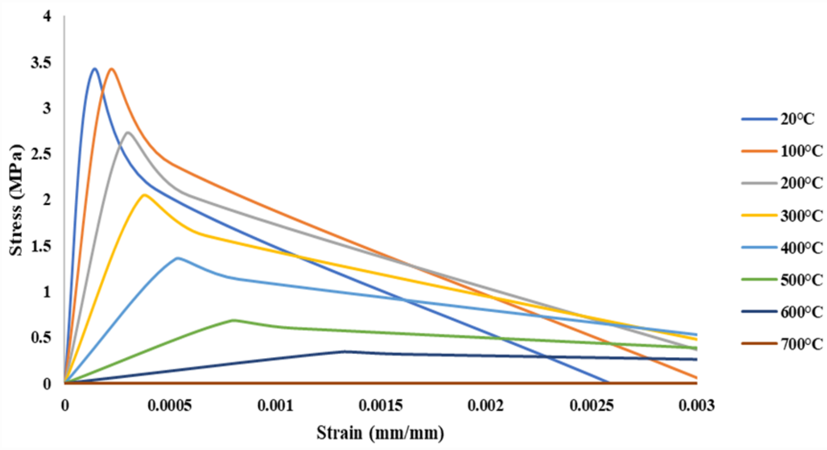

Figure 3: Concrete tensile stress-strain curves [41]

Under uniaxial tension, the concrete stress-strain response can be characterized by a linear elastic behaviour, followed by a softening branch, and finally a sudden brittle failure [34]. Although the concrete tensile strength is much lower than its compressive strength and is usually neglected in strength calculations, it is a significant property to consider in fire resistance. It can be a crucial property to consider in case of fire induced spalling. When concrete temperature reaches 300°C, it loses around 20% of its initial tensile strength. However, when it exceeds 300°C, the thermal damage in the form of microcracks is more pronounced, causing the tensile strength to decrease at a rapid rate [17]. Figure 4 displays the variation of the coefficient of thermal expansion with temperature which was adopted in this research.

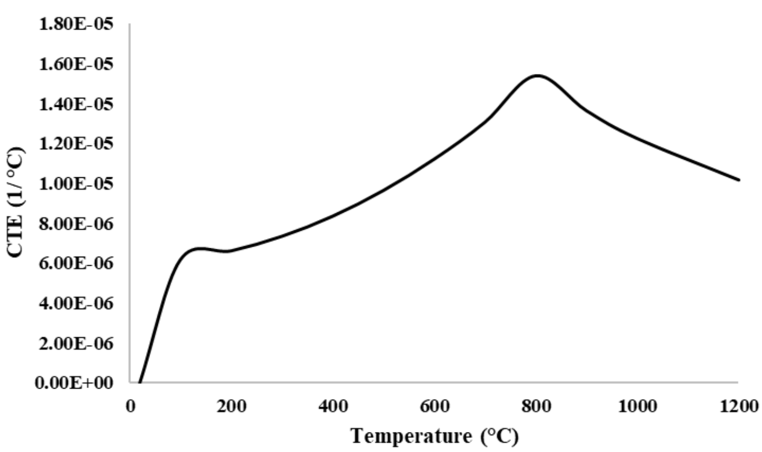

Figure 4: Concrete coefficient of thermal expansion variation with temperature [41].

The deformation of concrete under elevated temperatures was considered through the property of thermal expansion. In general, concrete expands when subjected to elevated temperatures, which induces thermal stresses. Therefore, thermal expansion is a significant property to consider and was assumed to vary with temperature according to relations provided by Eurocode 2 [41]. Initial concrete strengths of 30 and 50 MPa and Poisson's ratio of 0.2 were assumed.

3.1.1.2. Steel

3.1.1.2.1. Thermal properties of steel

The specific heat and thermal conductivity of the steel reinforcing bars were also assumed to vary with temperature. The variation of these properties was assumed according to Eurocode 3[42]

3.1.1.2.2. Mechanical and deformation properties of steel

Assuming an elastic-plastic behavior for steel bars, with or without strain hardening, is an acceptable approximation in modelling the steel reinforcing bars in RC structures [34]. Steel was assumed to have an elastic perfectly plastic behavior in both tension and compression as shown in Figure 5.

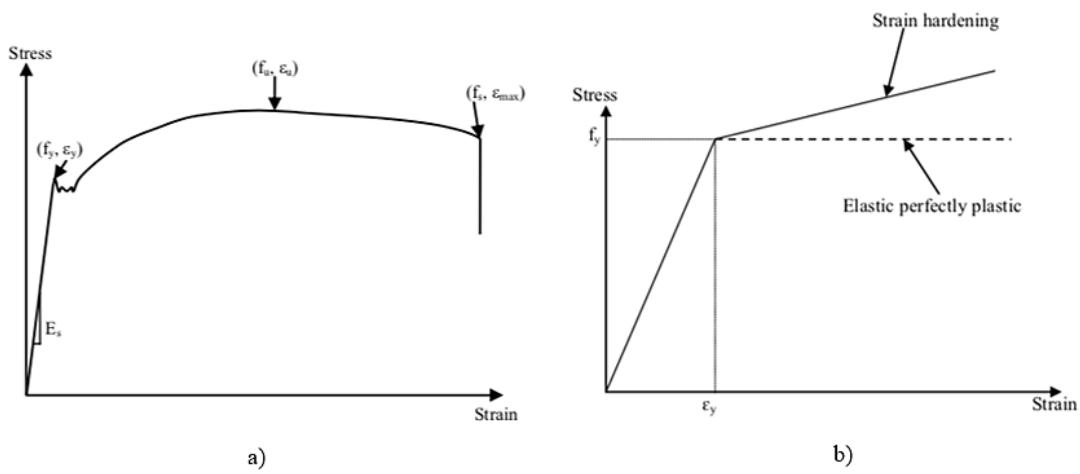

Figure 5: a) Typical and b) Idealized stress-strain curves for reinforcing steel[34].

The variation in the elastic modulus and yield stress of steel was input according to Eurocode 2, which provides stress-strain relationships for steel reinforcement corresponding to temperatures up to 1200 °C[41]. The initial Elastic modulus and yield strength was assumed to be 200 GPa and 520 MPa, respectively. A Poisson's ratio of

0.3 was assumed. The stress-strain curves that were adopted for steel are shown in Figure 6.

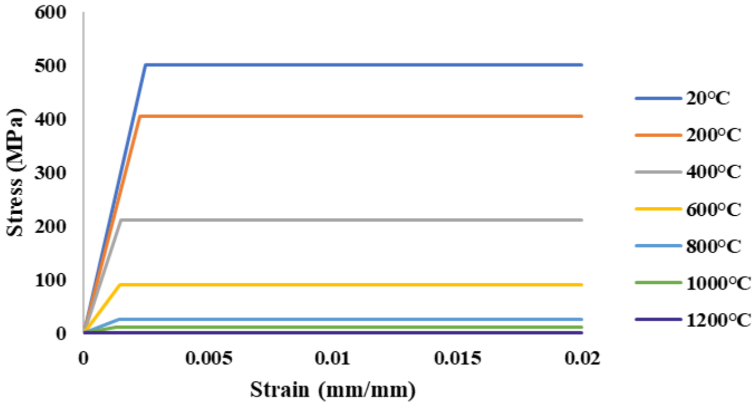

Figure 6: Steel stress-strain curves [41]

The coefficient of thermal expansion was also be assumed to vary with temperature and was input according to Eurocode 3 [42], as shown in Figure 7.

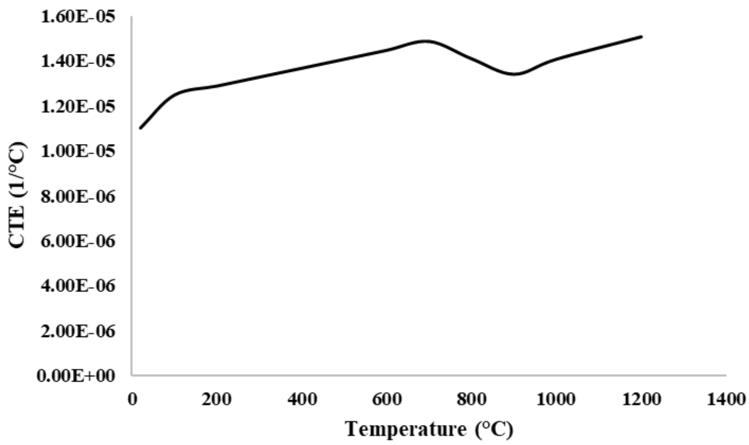

Figure 7: Steel coefficient of thermal expansion variation with temperature [42]

3.1.1.3. FRCM composite

3.1.1.3.1. Thermal properties of FRCM composite

The specific heat and thermal conductivity of the FRCM composite were input according to Cerny et al[43] and Anuar et al. [44] and were assumed to vary with the temperature. The density of the laminate was input according to George et al. [45] and was assumed not to vary with temperature exposure. According to the study, the densities of the PBO textile and the cement are 1560 and 1800 kg/m^3 respectively.

3.1.1.3.2. Mechanical properties of FRCM composite

The FRCM composite in the model was assumed to behave linearly elastic until failure. The initial properties of the PBO-FRCM are shown in Table 1 and were assumed according to Kyaure and Abed [34]. The strength and stiffness degradation were assumed to vary with the temperature according to Asgharigharakheili [26]. Given that the cementitious material has good compatibility with the concrete substrate, the FRCM and concrete were assumed to have perfect bond. To account for the FRCM confinement effect, the confined concrete compressive strength, f'_{cc} , was used in the model for the strengthened columns. It was calculated for each column using Equation 1 [46].

Table 1: FRCM Material Properties

Material Property	PBO Mesh	Cementitious Material	PBO FRCM Composite
Tensile Strength (MPa)	5800	-	1664
Compressive Strength (MPa)	-	30	-
Elastic Modulus (GPa)	270	6	128
Failure Strain (%)	2	-	1.7565
Nominal Thickness (mm)	0.05	-	

$$f'_{cc} = f'_c + 3.1\kappa_a f_l \,, \kappa_a = 1 \tag{1}$$

where:

f'_c *is concrete the compressive strength*

κ_a *is an efficiency factors based on the geometry of the cross section*

f_l *is the confinement pressure due to FRCM strengthening*

3.1.1.4. Fireproof insulation material

The fireproof insulation material for the columns was assumed to be a cement-based material, namely, Sikacrete 213F. This material was utilized in an experimental study by Khalaf et al. which will be discussed in detail in later the model verification. The thermal properties were input according to Mahdy et al. [35] The density, equal to 700 kg/m^3, was assumed to be constant. However, the thermal conductivity and specific heat were assumed to vary with temperature. Only the thermal properties of the insulation were considered since it was not expected to provide structural significance; therefore, it was excluded from the mechanical analysis.

3.1.2. Heat transfer analysis

An initial heat transfer model was conducted to obtain the element nodal temperatures for all heated columns. The thermal response of the columns was assessed using a transient heat transfer analysis in which heat flows from the surface of the column and spreads to its core. The heat transfer through the column surface was simulated through convection and radiation boundary conditions. The convective heat transfer coefficient (h_c) was taken as 25 $\frac{W}{m^2}K$. The absolute zero temperature (T_z) was taken as −273.15°C and the Stephan Boltzmann constant (σ) was taken as 5.67 ×10^{-8} $\frac{W}{m^2}K^4$. All specimens were heated following the ASTM E119 [23] standard fire temperature-time curve, which is shown in Figure 8, for a period of two hours. The concrete, FRCM, and steel reinforcement were assigned as DC3D8: 8-node linear heat transfer brick, DS4: 4-node heat transfer quadrilateral shell, and DC1D2: 2-node heat transfer link elements, respectively [36].

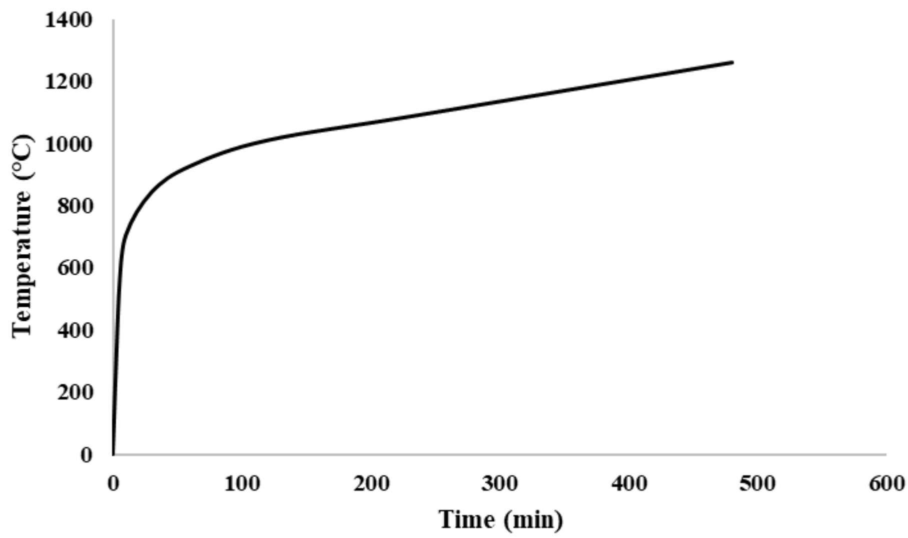

Figure 8: ASTM E119 temperature-time curve [23].

3.1.3. Mechanical response analysis

To evaluate the mechanical response of the columns subjected to elevated temperatures, a second finite model with two steps was developed. The first step was a static loading step in which the column was subjected to a preload determined as a percentage of its ultimate capacity. The capacity of each column was obtained using ABAQUS in a separate model in which the columns were loaded using a static, displacement-controlled loading step. The nodal temperatures from the initial heat transfer model were imported as a predefined field to a second static step, which represented the fire scenario. The preload value was maintained throughout the full analysis. The concrete and fireproof insulation, steel reinforcement, FRCM were assigned as C3D8R: 8-node linear brick with reduced integration, and T3D2: 2-node linear 3-D truss, S4R: 4-node shell with reduced integration elements respectively [34], [47].

3.1.4. Boundary conditions and constraints

In the heat transfer analysis, a surface film boundary condition was used to simulate convection. In the mechanical response analysis, all displacements were restrained at the columns ends. The steel reinforcement was constrained in the concrete using an embedded region constraint. To simulate the bond between the FRCM and the concrete, a tie constraint was used since a perfect bond was assumed between the concrete and the FRCM until failure. A tie constraint was also used to simulate the bond between the fireproof insulation and the concrete substrate for the unstrengthened columns; however, it was used to simulate the bond between the fireproof insulation and FRCM for the strengthened columns. In addition, tangential contact was used given the presence of end plates, which were added in the model to assure proper distribution of the load. The sustained point load was applied to the reference point on the top rigid plate.

3.1.5. Mesh configuration

Based on previous work by Kyaure and Abed [34], a mesh size of 20 mm for concrete and FRCM gave acceptable results. The steel was also given the same mesh size in the proposed model.

3.1.6. Model verification

The proposed FE model was used to simulate fire to several columns from different experiments. The chosen studies and obtained results will be discussed in this section.

3.1.6.1. Kodur et al.

The proposed thermal modeling approach was used to simulate fire exposure to a control, unstrengthened column, identified as Column 1, that was reported in published literature in a study by Kodur et al. [48] for verification. In this experimental study full-scale fire tests were performed on FRP-strengthened RC columns. Temperature-time curves obtained from ABAQUS[16] were compared to the experimental plots at two locations, one at a depth of 38 mm into the cross-section, and the other on one of the vertical steel bars. The thermal properties vs. temperature for concrete and steel were input according to Eurocode 2 [41] and Eurocode 3[42] respectively.

3.1.6.2. Chowdhury et al.

Another study by Chowdhury et al. [27] was selected to verify the proposed FE approach. Full scale fire tests were conducted on 2 FRP-strengthened RC circular columns to study the effect of insulation on their fire performance in the selected experimental study, both of which were modeled using ABAQUS [16]. The first column, identified as Column 3, is a column strengthened with 2 layers of FRP without insulation (control) and the second column, identified as Column 4, is a replicate of Column 3, but with an insulation layer. For both columns, FE temperature-time curves were compared to the experimental temperature-time curves at three different locations: at a depth of 50 mm into the concrete, at a depth of 100 mm into the concrete, and the longitudinal reinforcement. The variation of thermal properties for the concrete and steel were assumed according to Eurocode 2 [41] and Eurocode 3 [42] respectively. The thermal properties of the FRP and insulation materials were assumed according to Mahdy et al. [35] in which numerical verification was performed for the same columns using ANSYS FE software[49].

3.1.6.3. Experiments on FRP- and FRCM- strengthened RC columns

Full-scale fire tests have been performed by Khalaf et al. on circular RC columns with the details shown in Figure 9. The columns varied in the type of strengthening (PBO-FRCM and CFRP) and the presence of fire proofing insulation. The fireproofing material was a cement-based system, Sikacrete-213F. Selected columns from the study were modelled with the details mentioned in Table 2. FE temperature-time curves were verified against the experimental results at three locations in the cross-section: concrete surface, near the longitudinal reinforcement, and concrete core, which are labelled in Figure 10 as 4, 3, and 1 respectively. The variation of the thermal properties with temperature for the concrete and the steel were also assumed according to Eurocode 2 [41]and Eurocode 3 [42]respectively. The variation of the thermal properties of the FRCM laminate were assumed according to the studies mentioned earlier in section

3.1.1.2.3. For the CFRP laminate, the density was also assumed to be constant and was input according to the carbon fibre datasheet provided by the manufacturer[50]. The specific heat and thermal conductivity of the fireproofing material were assumed to vary with temperature and were input according to the previously mentioned study in section 3.1.6.2.

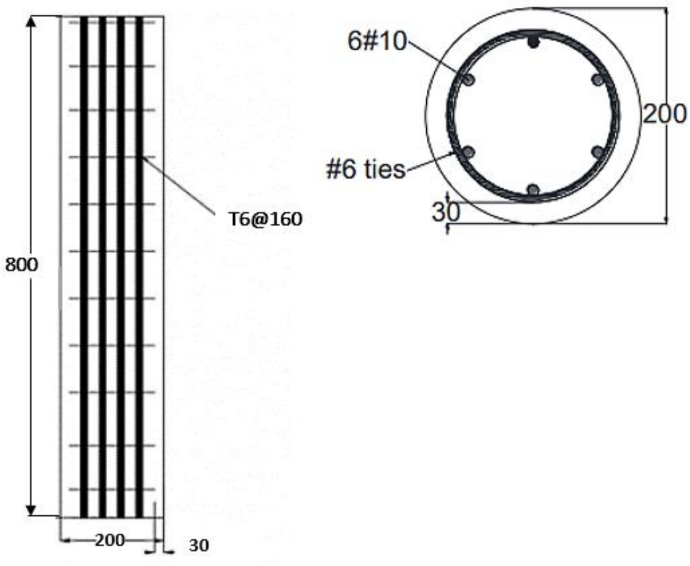

Figure 9: Column dimensions (all dimensions are in mm).

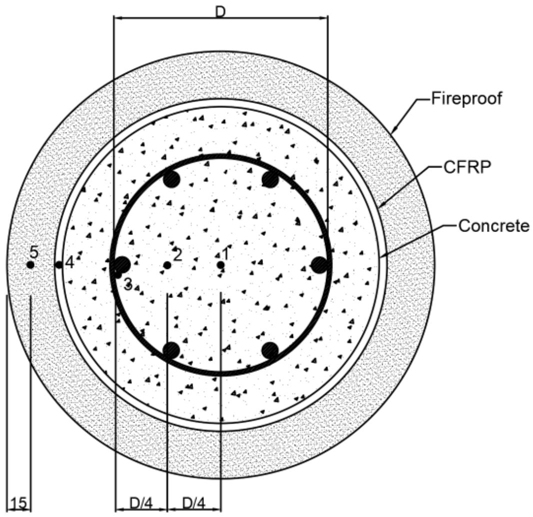

Figure 10: Thermocouple locations in the column cross-section.

Table 2: Details of Modeled Columns

Specimen ID	Strengthening System	Number of Layers	Thickness of Fireproof Layer (mm)
Control	-	-	-
Control-FP	-	-	30
PBO-1-A	PBO FRCM	1	-
PBO-2-A	PBO FRCM	2	-
PBO-4-A	PBO FRCM	4	-
PBO-2-A-FP	PBO FRCM	2	30
C-2-FP	CFRP	1	30

3.1.6.4. Results and discussion

Figure 11 displays the temperature-time curves for Column 1 in the previously discussed study by Kodur et al. [48]. The FE temperature-time curves were in close agreement with those of the experiments, until approximately 2 hours of fire exposure, after which temperature variation started to be observed. The calculated percentage differences between the FEA results and the experimental results after 4 hours of fire exposure were 14% and 15.5% for the maximum temperatures reached at the first and second location, respectively. There was an overall close agreement between the FE and experimental results for this column; however, the variation of temperature that started to occur led to a difference in the final temperatures reached. Since the proposed heat transfer FE model did not account for possible cracks in the concrete, this possibly resulted in underestimation of the final reached temperatures in the FE model.

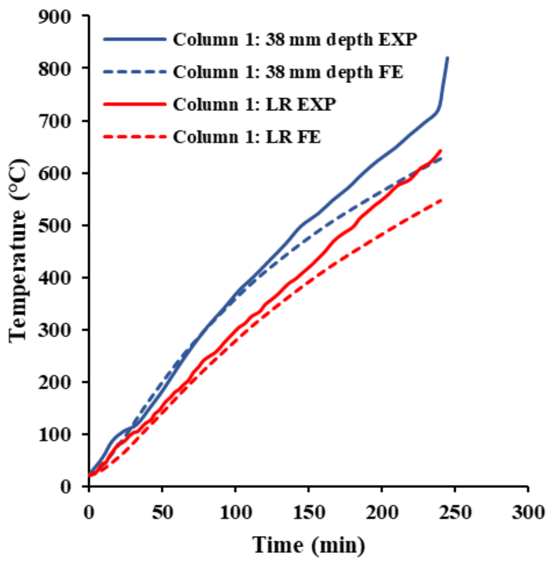

Figure 11: Kodur et al. verification [48].

The temperature-time plots for Columns 3 and 4 in the study by Chowdhury et al. [27]are shown in Figure 12. For Column 3, the strengthened, uninsulated column, it can be observed that the obtained FE results were in close agreement with those of the experimental results with percentage differences of 4 and 6% for the maximum temperatures reached at 50 and 100 mm depths into the concrete respectively. For Column 4, the strengthened, insulated column, the closest agreement between the FE and the experimental results was observed at a depth of 50 mm into the concrete cross-section. At a depth of 100 mm, the FE final temperature was almost identical to that obtained from the fire test.

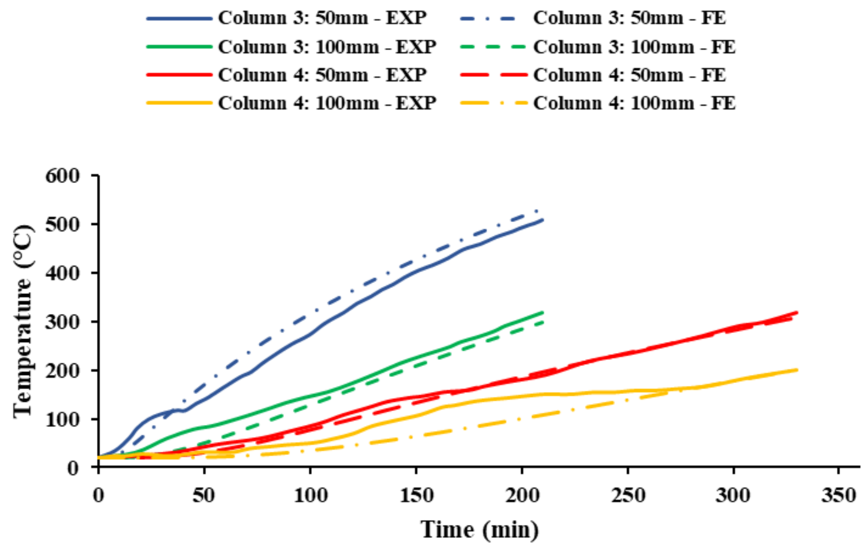

(a)

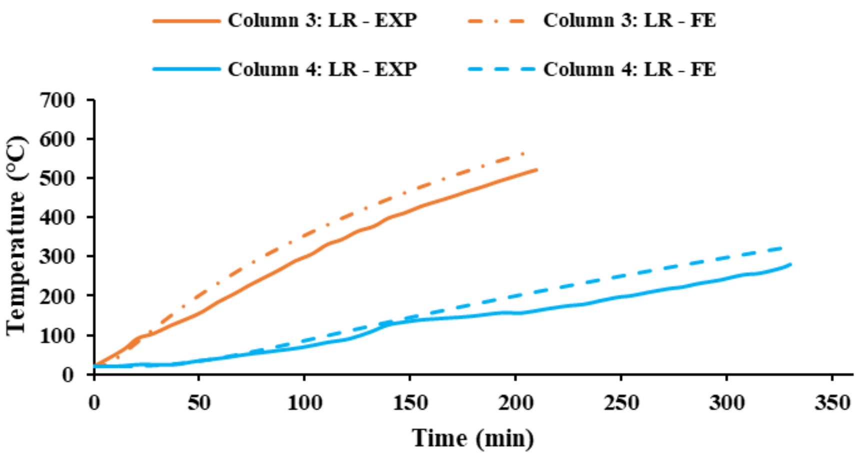

(b)

Figure 12: Chowdhury et al. [27] verification for (a) Concrete and (b) Longitudinal reinforcement.

However, a gradual variation occurred after around 1.5 hours of fire exposure. A maximum difference of 50 % was observed at the 3-hour mark. As mentioned earlier, the FE model did not account for concrete cracks, which possibly resulted in underestimation of the predicted concrete temperature in some cases. After exceeding the 3-hour duration, there was close agreement between the FE and experimental results.

A difference of 10% was observed at the longitudinal reinforcement with overestimation in the FE temperatures. Comparing the longitudinal reinforcement temperature-time curves until 2.5 hours of exposure, very similar behavior was shown between the FE and the experimental results, after which the temperatures started to vary and reached a difference of approximately 15%. Overall, the predicted temperature-time curves agreed well with the experimental ones, with the FE results on the more conservative side.

For the PBO- and FRP- strengthened columns, the temperature-time verification is presented in Figures 13-16. Figure 13 represents the plots for columns Control and Control-FP. Overall, the FE plots agreed well with the experimental ones; however, there were some variations since the heat transfer model did not account for all the possible scenarios in the experiments. For example, when comparing the surface plots for Control-FP, there was close agreement between the FE and experimental final reached temperatures before the jump that occurred in the experimental plot at the 2-hour mark. This occurred due to spalling of the fireproof layer of the column, which was not accounted for in ABAQUS [16]. Moreover, when observing the center plots for the Control column, a temperature diversion started to occur after approximately 1 hour of fire exposure. A final difference of 22% was reached with underestimation in the predicted final reached temperature. This might have occurred due to cracks in the concrete which were also not accounted for in the model.

Moving on to the FRCM-strengthened columns, Figure 14 shows the FE and experimental plots for columns PBO-1-A and PBO-4-A. For the surface plots of PBO-1-A, there was close agreement between the experimental and predicted temperatures until the jump in the experimental plot that occurred after around 40 minutes of fire exposure, at which the spalling of the FRCM layer was assumed to occur. The same jump occurred for the center plots of the same column before which there was good agreement between the predicted and numerical temperatures. Due to possible cracks or concrete spalling that were not accounted for in the finite element model, the sudden temperature rise occurred in the central plot. For column PBO-4-A, the surface plots were in close agreement until the cut that occurred in the experimental plot after 1 hour of fire exposure due to meaningless thermocouple readings.

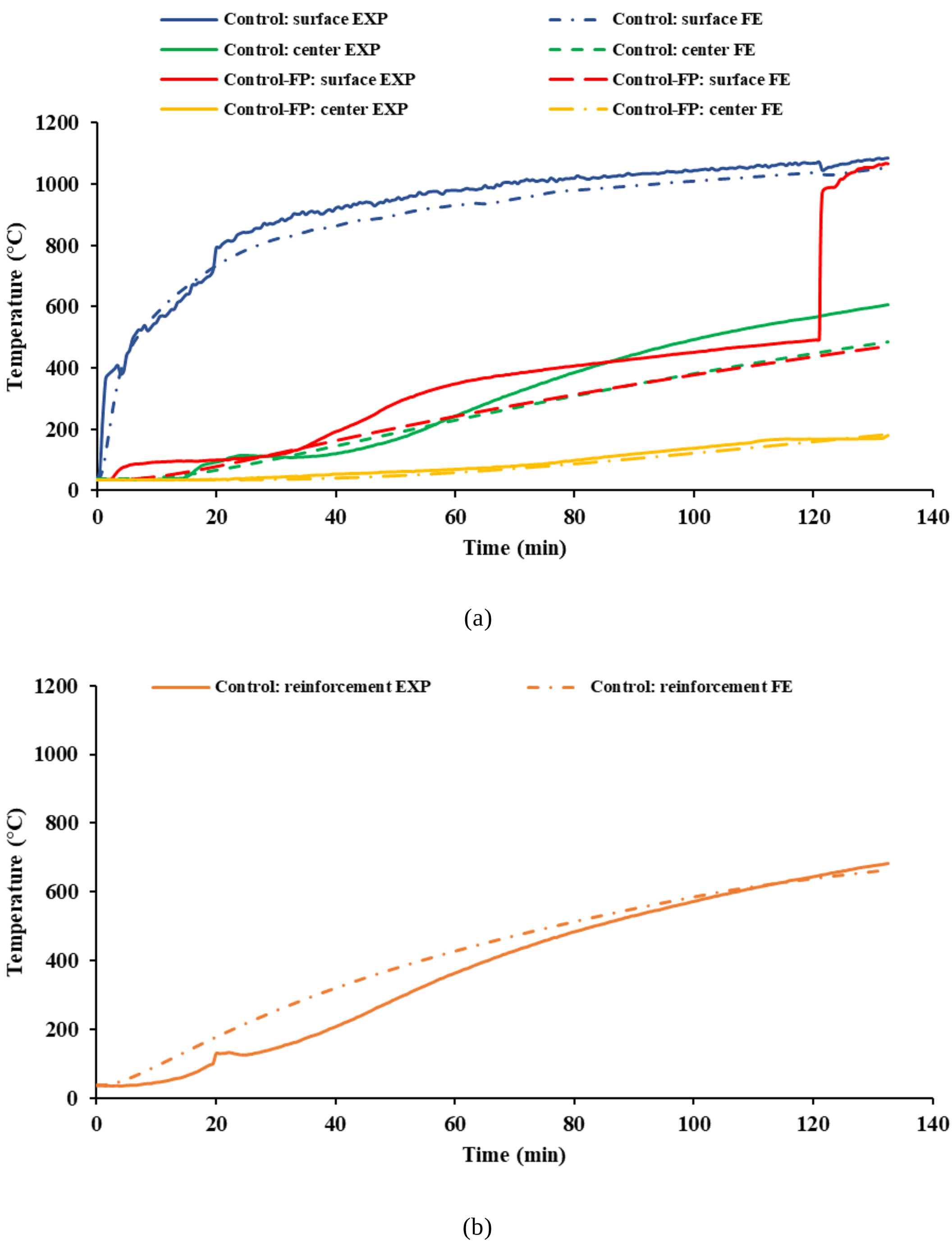

Figure 13: Control and Control-FP verification for (a) Concrete and (b) Longitudinal reinforcement.

When comparing the central plots, the same observation can be made as for the central plots of column PBO-1-A. An experimental temperature jump occurred after around 1 hour and 10 minutes of fire exposure, possibly due to the previously mentioned reasons.

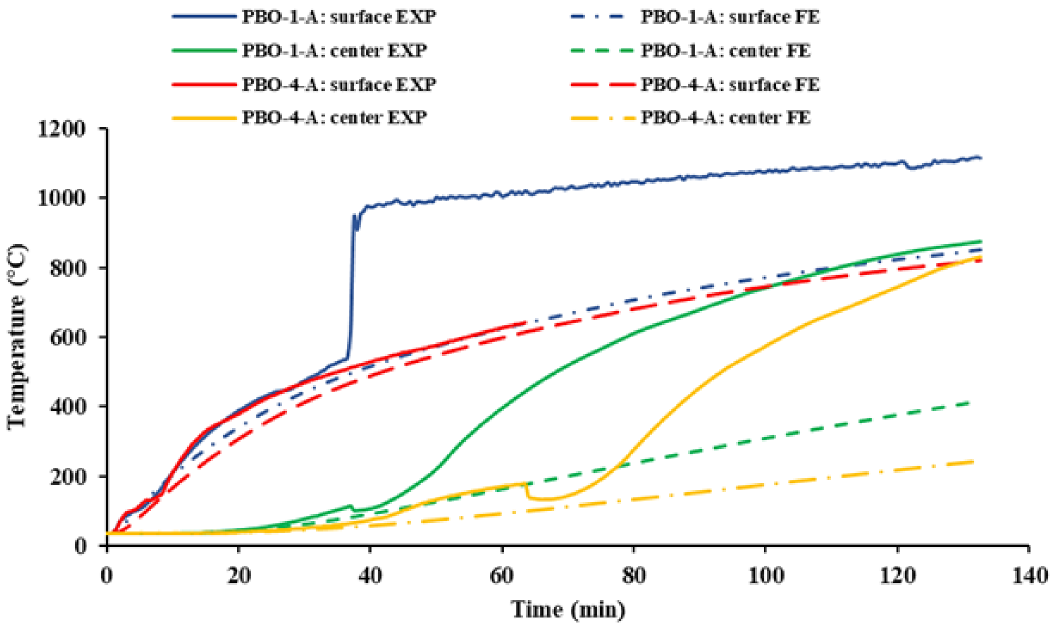

(a)

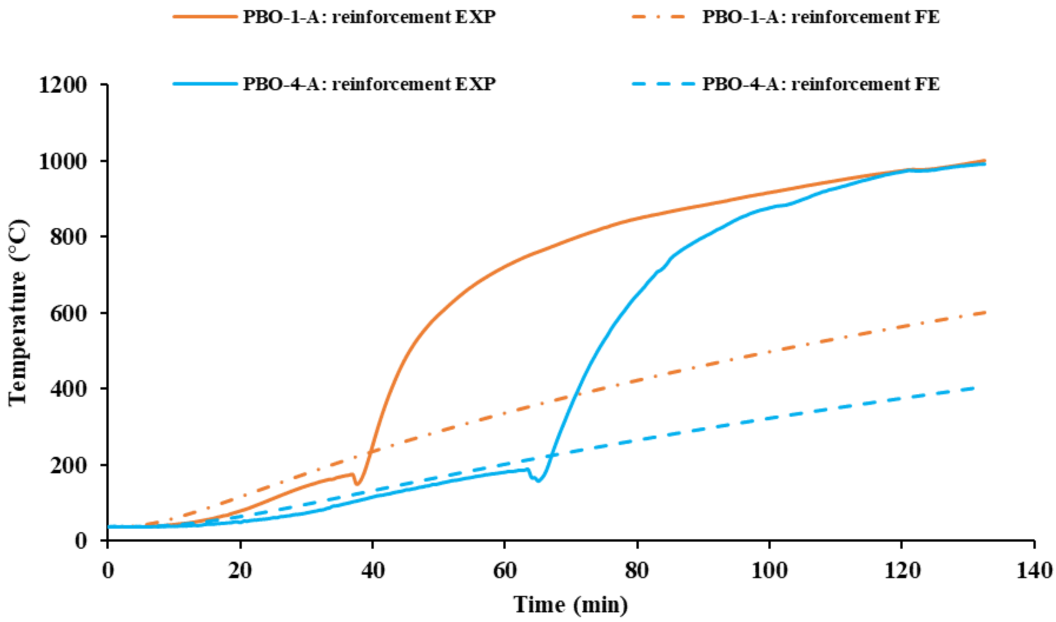

(b)

Figure 14: PBO-1-A and PBO-4-A verification for (a) Concrete and (b) Longitudinal reinforcement.

For both the reinforcement plots of PBO-1-A and PBO-4-A, there were jumps that occurred after approximately 40 minutes and 1 hour of fire exposure, respectively, in the experimental plots due to the previously discussed points that also affected the reinforcement temperatures.

The plots for columns PBO-2-A and PBO-2-A FP are represented in Figure 15. When comparing the concrete surface temperature-time curves for column PBO-2-A, the same scenario for column PBO-1-A can be observed.

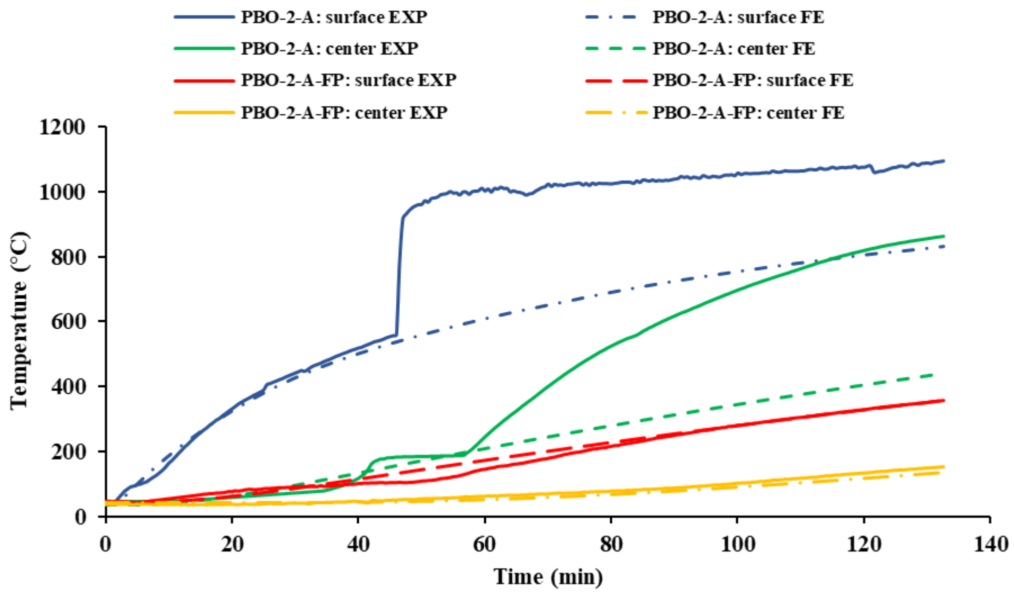

(a)

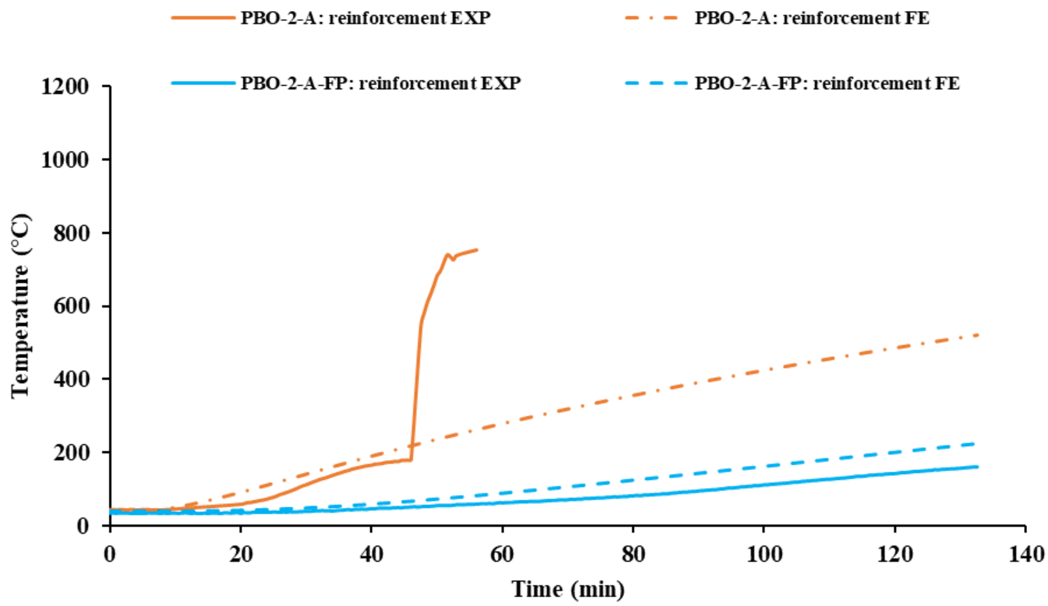

(b)

Figure 15: PBO-2-A and PBO-2-FP verification for (a) Concrete and (b) Longitudinal reinforcement.

There was close agreement between the FE and experimental temperatures until around 45 min of exposure, afterwhich a significant jump occurred in the experimental curve due to spalling of the FRCM layer. The same occurred for the center curves of the same column, probably due to exposure of the central thermocouple as a result of concrete cracking or spalling. On the other hand, the FE and experimental temperature time curves were almost identical at the concrete surface and center locations for column PBO-2-A-FP.

Comparing the reinforcement temperature-time curves, the previously discussed jump in the experimental temperatures was observed for column PBO-2-A due to concrete spalling. For PBO-2-A-FP, the FE plots agreed well with the experimental ones. The plots had a very similar behavior with conservative predicted temperatures. The percentage difference between the experimental and predicted final reached temperature was around 33%.

Finally, the experimental and predicted temperature plots for the FRP-strengthened column C-2-FP are shown in Figure 16. Due to possible spalling of the fireproof layer, there were spikes in the experimental temperatures. This led to higher experimental temperatures in certain ranges compared to the FE predicted ones. Moreover, a jump was also observed in the center experimental plot after 1 hour and 15 minutes of exposure.

This was possibly due to the initial spalling of the fireproof layer, which led to the exposure of the central thermocouple. When observing the reinforcent plot, there was close agreement between the FE and experimental temperatures, up until the drop that occurred in the experimental plot after approximately 1 hour and 30 minutes of fire exposure.

Overall, conservative or underestimated temperature were predicted due to several possible reasons. Firstly, the proposed FE model did not account for material cracks, fire-induced spalling, and many other scenarios that possibly occurred during the experiments.

Moreover, the actual initial thermal material properties of those in the experimental specimens were not all available by the manufacturer. In addition, even if these initial properties were available, their variation with temperature was not exactly known.

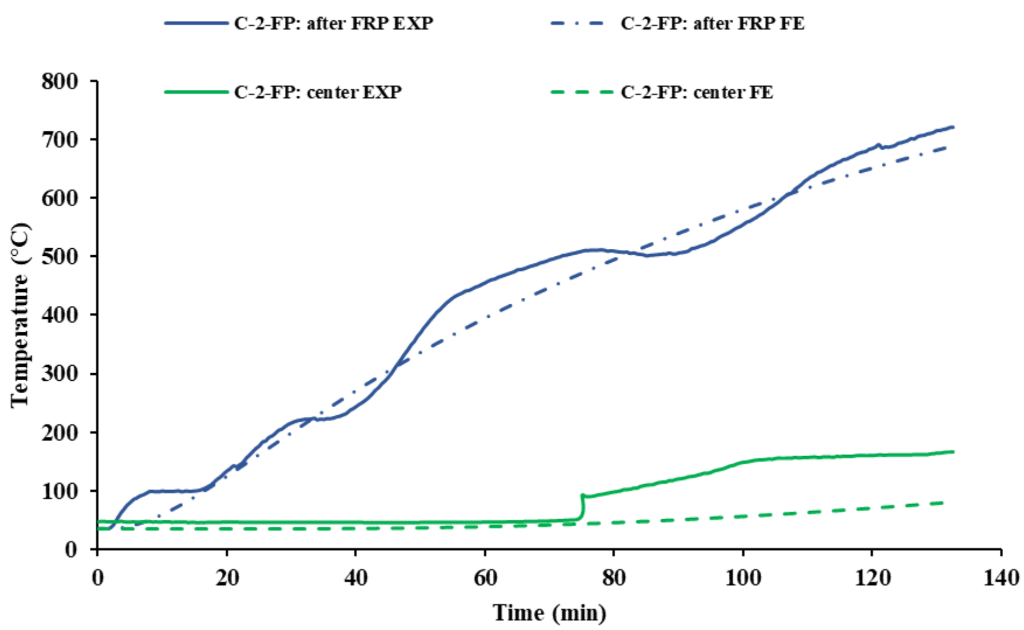

(a)

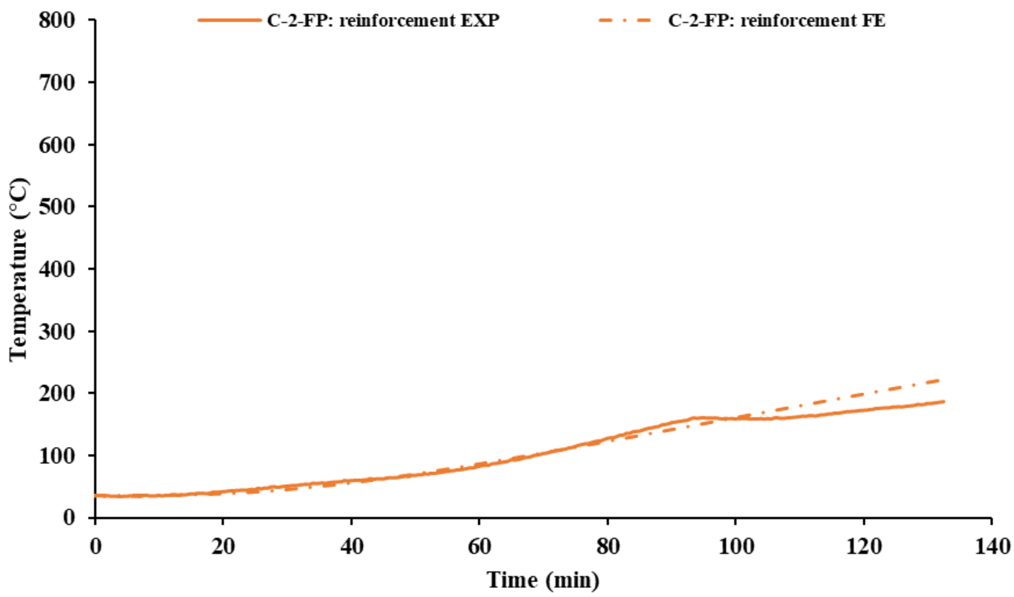

(b)

Figure 16: C-2-FP verification for (a) Concrete and (b) Longitudinal reinforcement.

Chapter 4. Finite Element Analysis of PBO FRCM- Strengthened Columns

In this chapter, the parametric study conducted is discussed in detail. Moreover, the FE results are presented using terms of load and displacement -time curves along with the detailed analysis. In addition, the temperature and Von Mises stress contours are discussed.

4.1. Parametric Study

A parametric study was conducted to investigate the parameters that most affected the performance of unconfined and PBO FRCM – confined columns. The parameters considered in the current study comprised the concrete cover (40, 50, and 60 mm), the number of PBO FRCM layers (0, 1, and 2), the presence of a 30 mm thick insulation layer, and the applied axial load. All the modeled columns were short columns with a circular cross section with a fixed core diameter (140 mm) and a length of 800 mm. The columns were reinforced with 6#12 longitudinal bars and 5#6 ties at spacing of 160 mm. Figure 17 shows the elevation and cross section of the modeled columns.

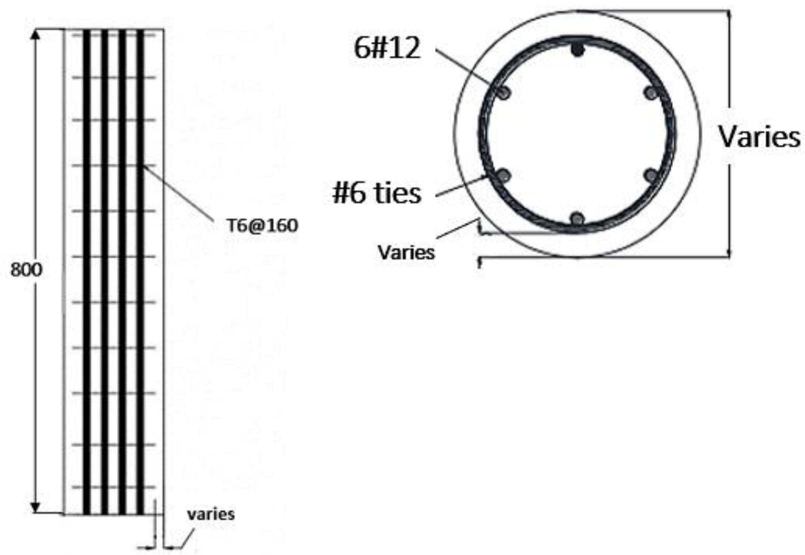

Figure 17: Column details used in the FE model (all dimensions are in mm).

4.2. Test Matrix

The test matrix of this study comprises 36 columns. Each column was modeled over 2 stages. The first stage consisted of a thermal model whose output was used in a second mechanical model. The specimens were divided into 4 series with each focusing on a certain parameter. Each series is discussed in the following sections. The specimen identification is presented in Figure 18.

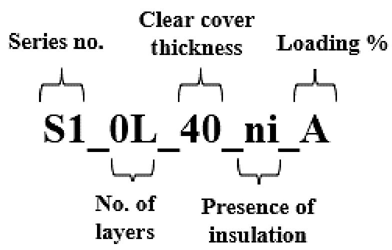

Figure 18: FE specimen identification.

The first part of the specimen's identification refers to the series number (1, 2, 3A, 3B, or 4), the second part indicates the number of FRCM layers used (0, 1, or 2 layers), the third part represents the concrete clear cover (40, 50, or 60 mm), the fourth part indicates the presence of insulation (*ni* for non-insulated specimens and *i* for the insulated ones), and the final part denotes the % of the ultimate capacity that is applied to the column under consideration.

4.2.1. Specimens loaded with a fixed load

To investigate the effect of the number of FRCM layers, 9 columns were modelled and grouped in Series 1 as listed in Table 3.

Table 3: Series 1

Specimen ID	Number of Layers	Clear Cover Thickness (mm)	Thickness of Insulation (mm)	Applied Load (kN)
S1_0L_40_ni_A	0	40	-	625
S1_1L_40_ni_A	1	40	-	625
S1_2L_40_ni_A	2	40	-	625
S1_0L_40_ni_B	0	40	-	938
S1_1L_40_ni_B	1	40	-	938
S1_2L_40_ni_B	2	40	-	938
S1_0L_40_ni_C	0	40	-	1173
S1_1L_40_ni_C	1	40	-	1173
S1_2L_40_ni_C	2	40	-	1173

In this series, the capacity of the unstrengthened column was obtained using a displacement-controlled model that was developed using ABAQUS. The columns of Series 1 were then grouped based on the applied axial load taken as a percentage of the unstrengthened column capacity (40, 60, and 75%), which are referred to as A, B, and C in the specimen identification, respectively. For example, column S1_2L_40_ni_A, refers to a column in series 1 that is strengthened with 2 layers of PBO FRCM systems without any insulation layer and loaded with 625 kN (40% of the unstrengthened column capacity).

4.2.2. Specimens loaded with variable loads

Series 2 consists of 9 columns to investigate the effect of the applied axial load taken as a percentage of the capacity of the specimen of interest rather than a fixed load. The difference between the columns of this series and those of series 1 lies in the applied axial load. The aim of this series was to study the column performance when increasing the applied load as a percentage of its own capacity. The letters A, B, and C in this series represent 40, 60, and 75% of the ultimate capacity of the tested column. Table 4 presents the details of the specimens in Series 2.

Table 4: Series 2

Specimen ID	**Number of Layers**	**Clear Cover Thickness (mm)**	**Thickness of Insulation (mm)**	**Applied Load (kN)**
S2_0L_40_ni_A*	0	40	-	625
S2_0L_40_ni_B*	0	40	-	938
S2_0L_40_ni_C*	0	40	-	1173
S2_1L_40_ni_A	1	40	-	745
S2_1L_40_ni_B	1	40	-	1118
S2_1L_40_ni_C	1	40	-	1398
S2_2L_40_ni_A	2	40	-	868
S2_2L_40_ni_B	2	40	-	1303
S2_2L_40_ni_C	2	40	-	1628
* Indicates specimens repeated from Series 1				

For example, S2_1L_40_ni_A, S2_1L_40_ni_B, and S2_1L_40_ni_C were loaded with 747, 1118, and 1398 kN, which represent 40, 60, and 75% of the capacity of a column strengthened with one layer of PBO FRCM respectively.

4.2.3. Specimens with various concrete clear covers

The concrete clear cover acts as a protection barrier to the columns' reinforcement when the column is exposed to fire. The fire performance of columns with concrete clear covers of 40, 50, and 60 mm were investigated and compared. Columns of series 3A and 3B consist of column with 50 and 60 mm covers, respectively, and loaded with 60 and 75% of their capacity. The details of these two series are shown in Table 5.

Table 5: Series 3A and 3B

Specimen ID	Number of Layers	Clear Cover Thickness (mm)	Thickness of Insulation (mm)	Applied Load (kN)
S3A_0L_50_ni_B	0	50	-	938
S3A_0L_50_ni_C	0	50	-	1173
S3A_1L_50_ni_B	1	50	-	1118
S3A_1L_50_ni_C	1	50	-	1398
S3A_2L_50_ni_B	2	50	-	1303
S3A_2L_50_ni_C	2	50	-	1628
S3B_0L_60_ni_B	0	60	-	938
S3B_0L_60_ni_C	0	60	-	1173
S3B_1L_60_ni_B	1	60	-	1118
S3B_1L_60_ni_C	1	60	-	1398
S3B_2L_60_ni_B	2	60	-	1303
S3B_2L_60_ni_C	2	60	-	1628

4.2.4. Specimens with and without insulation

The presence of an insulation layer can substantially affect the fire performance of the columns since it delays the temperature rise in the cross section. Although FRCM systems have the potential to improve the fire performance of the strengthened columns, it is important to investigate the difference in the fire performance of those columns when an insulation layer is applied. Series 4 comprises columns that are identical to those of Series 2 but with a 30 mm layer of insulation layer. Table 6 presents the details of those specimens.

Table 6: Series 4

Specimen ID	Number of Layers	Clear Cover Thickness (mm)	Thickness of Insulation (mm)	Applied Load (kN)
S4_0L_40_i_A	0	40	30	625
S4_0L_40_i_B	0	40	30	938
S4_0L_40_i_C	0	40	30	1173
S4_1L_40_i_A	1	40	30	745
S4_1L_40_i_B	1	40	30	1118
S4_1L_40_i_C	1	40	30	1398
S4_2L_40_i_A	2	40	30	868
S4_2L_40_i_B	2	40	30	1303
S4_2L_40_i_C	2	40	30	1628

4.3. Results and Discussion

A total of 36 columns were modeled to investigate their fire performance when exposed up to five hours of ASTM E119[23] standard fire. As mentioned earlier, all columns were subjected to static axial loads corresponding to either constant loads (columns of series 1) or percentages of their axial capacity (columns of Series 2 to 4), which were maintained during fire exposure. The effect of each of the investigated parameters on the performance of the columns is analysed and discussed in the following sections.

4.3.1. Thermal response of the tested columns

Temperature-time curves have been extracted at 3 different locations of the specimen's cross section for selected modeled columns. For the unstrengthened columns, the temperature-time curves are shown at the level of the concrete surface, the level of the steel reinforcement, and the middle of the concrete core. For the strengthened columns, the temperature-time curves are shown at the level of the FRCM surface, the level of the steel reinforcement, and the middle of the concrete core. The temperature-time curves are shown in Figure 19.

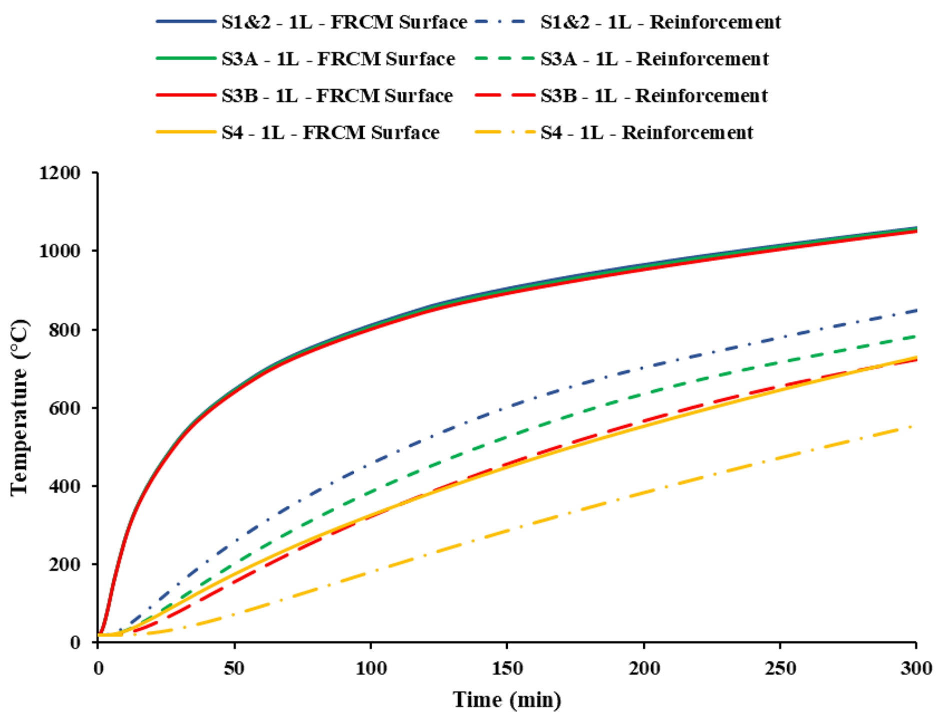

(a)

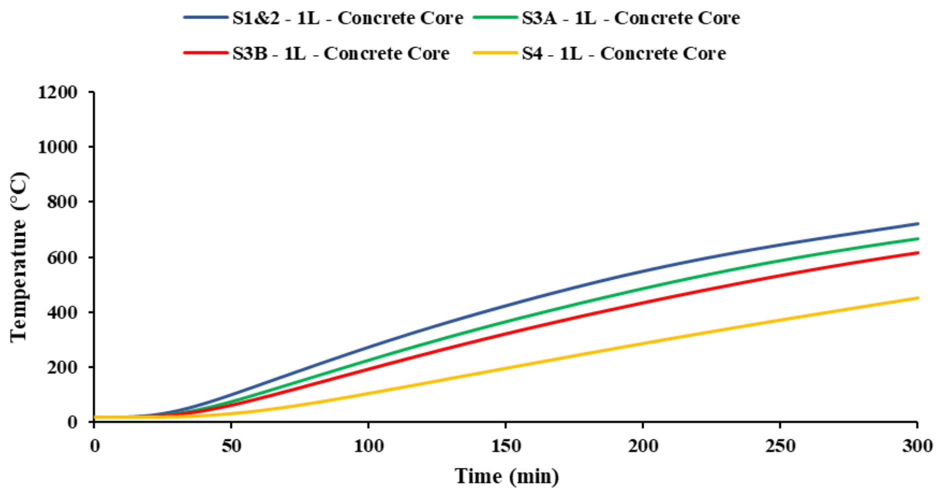

(b)

Figure 19: Temperature-time curves for (a) FRCM Surface and level of steel and (b) Concrete core.

Perfect bond was assumed between the FRCM layer and the concrete substrate. Moreover, it is important to note that the thermal model did not account for the FRCM rupture or the fire induced spalling of concrete. For columns of series 1 and 2 (with a concrete clear cover of 40 mm), the same thermal models were used since those columns were only distinct during the mechanical analysis stage where the applied load was changed.

Figure 19 compares between the temperature-time curves for columns of series 1, 2, 3A, 3B, and 4 strengthened with one layer of FRCM. As anticipated, the temperatures measured at the FRCM surface were almost identical for the columns in Series 1, 2, and 3A, and 3B. Moreover, the temperatures measured at the level of the steel reinforcement were considerably lower than those at the FRCM surface for all columns, which is attributed to the low thermal conductivity of concrete that acted as a protection layer for the steel reinforcing bars. Since the FRCM was applied as a shell element with a relatively thin thickness, it was not expected to act as an insulation layer. When comparing the reinforcement temperature-time curves of the columns with 50 and 60 mm concrete covers (Series 3A and Series 3B) to those of their counterparts with a 40 mm cover (Series 1 and Series 2) in Figure 19, we can conclude that increasing the cover thickness significantly decreased the temperature at every point in time.

Figure 20 shows the recorded temperatures at the level of the steel reinforcement after different fire exposure periods for the columns strengthened with 1 layer of FRCM having 40, 50, and 60 mm concrete clear covers (columns of Series 2, 3A, and 3B respectively).

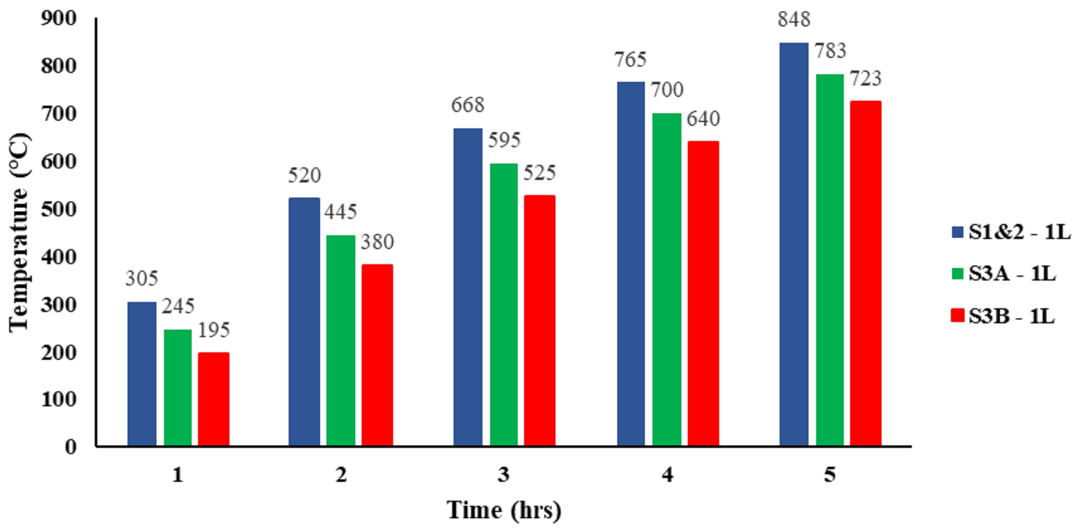

Figure 20: Temperatures at the level of reinforcement.

The temperatures at the level of the steel bars were recorded after 1, 2, 3, 4, and 5 hours of fire exposure for the columns in Series 1, 2, 3A, and 3B. For each of these durations, it can be noticed that the corresponding temperatures decreased as the concrete cover thickness increased. For instance, after 1 hour of fire exposure, the recorded temperatures were 500, 445, and 380°C for columns with 40, 50, and 60 mm covers respectively. Therefore, increasing the cover to 50 mm (columns of series3A) led to a 14% drop in the temperature at the level of the steel bars whereas increasing it to 60 mm (columns of series 3B) decreased the temperature at the level of the steel bars by 27%.

Moving on to the columns of Series 4, it is evident from the temperature-time curves of the FRCM, steel, and concrete core in Figure 19 that the insulation significantly reduced the temperatures throughout the whole cross section. Figure 21 **s**hows the temperatures at the FRCM surface, the level of the steel reinforcement, and middle of the concrete core after fire exposure of 1, 2, 3, 4, and 5 hours for the columns strengthened with 1 layer of FRCM in Series 4. The temperatures at the same locations for the columns of Series 1 and 2 are also shown for comparison. A considerable drop in temperature at all considered levels through the cross section was noticed in columns of series 4. However, the % of drop in temperature compared to the columns of Series 1 and 2 decreased over the fire exposure duration. For example, the percentage drop in temperature after 1 hour of fire exposure was around 70% at the FRCM surface for the insulated column compared to 30% for the same column after 5 hours of exposure. This finding was also observed at the steel and concrete core levels. Although the binding matrix for FRCM is cement-based (unlike the organic epoxy resins used in FRP), these results demonstrated the need of insulation even though the cement-based matrices have a potentially improved fire resistance.

To demonstrate the effect of insulation on the columns' performance when the columns are loaded, the temperature contour for columns S2_1L_40_ni_B and S4_1L_40_i_B recorded shortly after failure are shown in Figure 22. S2_1L_40_ni_B failed after around 65 minutes of fire exposure whereas S4_1L_40_i_B failed after a duration of around 215 minutes. The insulation was successful in delaying the heat rise in all regions of the cross section as shown in Figure 22.

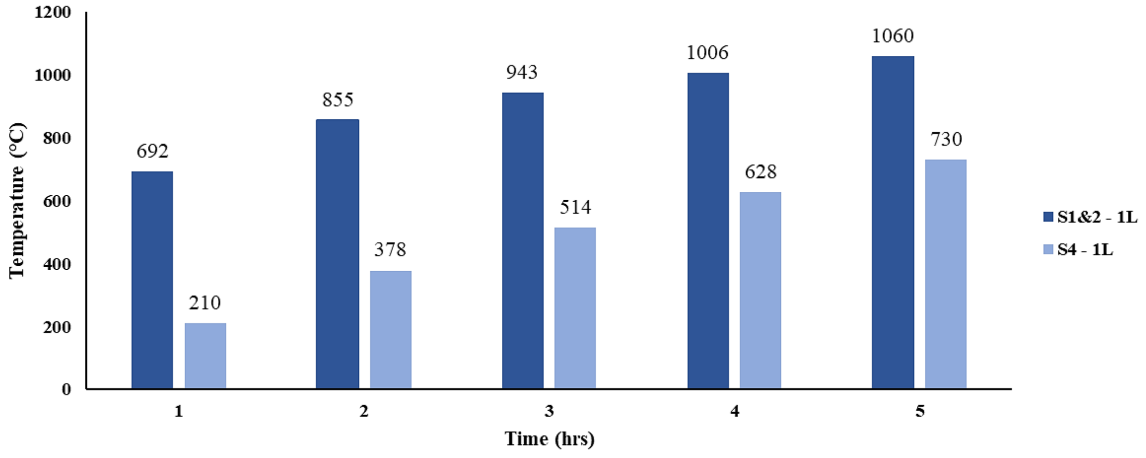

(a) FRCM Surface

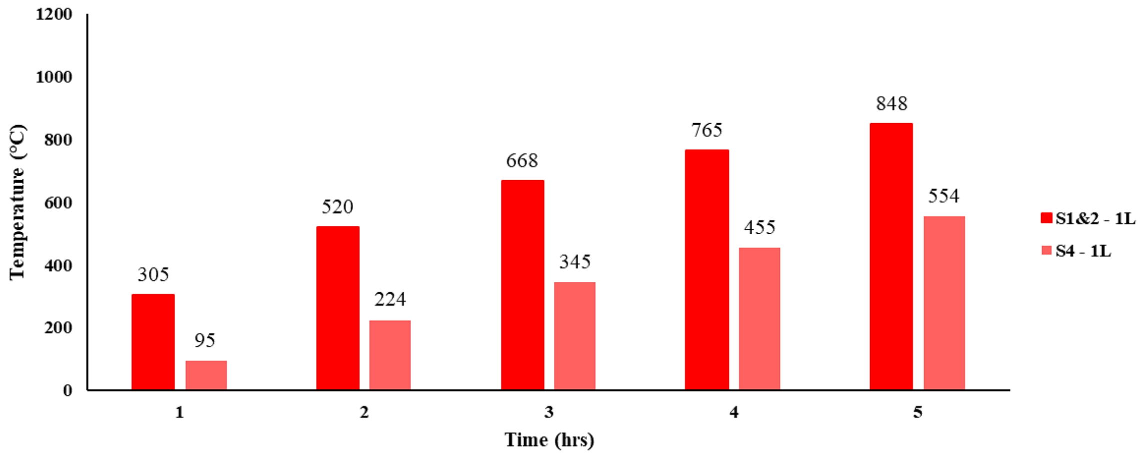

(b) Level of Reinforcement

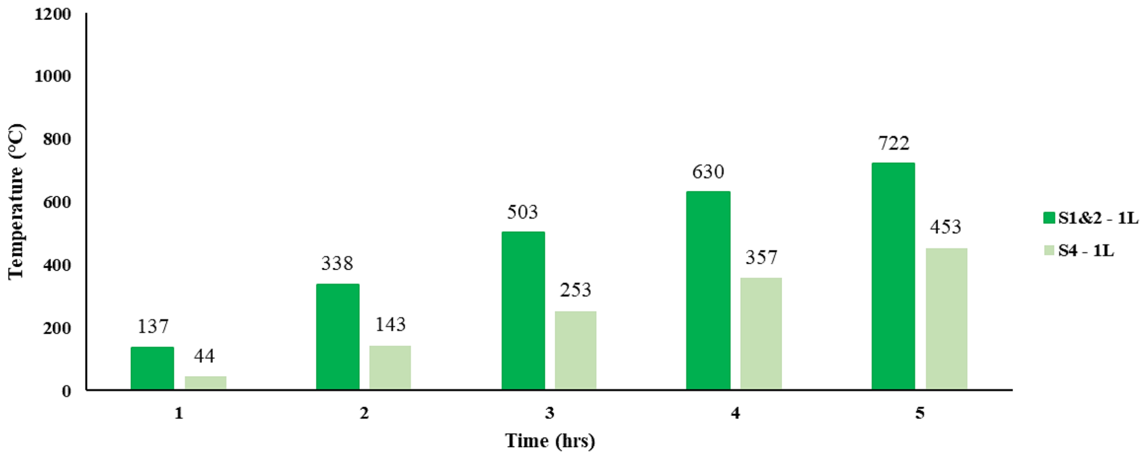

(c) Concrete Core

Figure 21: Temperatures at Different Levels of the Cross Section.

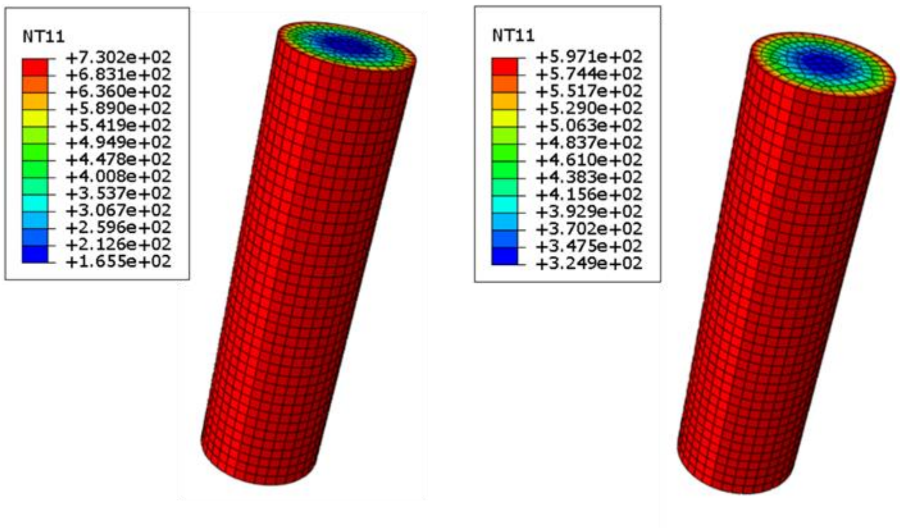

(a) S2_1L_40_ni_B (b) S4_1L_40_i_B

Figure 22: Temperature contours.

4.3.2. Mechanical response of the tested columns

The mechanical response of the modeled columns was evaluated using load-time and displacement-time plots as detailed in the following subsections. The effect of the previously mentioned parameters on the mechanical behavior of the columns are also discussed.

4.3.2.1. Effect of number of FRCM layers

To study the effect of wrapping the columns with FRCM layers on their fire performance, 3 fixed loads were applied to the specimens in Series 1 corresponding to 40, 60, and 75% of the load-carrying capacity of their control unstrengthened column. A load of 625 kN was applied to S1_0L_40_ni_A, S1_1L_40_ni_A, and S1_2L_40_ni_A and their load-time and deformation-time plots are shown in Figure 23-a. The sustained load was applied to the specimens during the fire exposure until failure was observed. The failure criteria for all columns was selected according to ASTM E119 [23] standards, which classifies the column based on the time in which it can sustain the applied load.

The unstrengthened column, S1_0L_40_ni_A, failed after 65 minutes of fire exposure. At that point, the temperature of the longitudinal steel reinforcement reached around 335°C indicating that it had lost more than 40% of its yield strength while the temperature of the concrete core reached approximately 160°C. According to Eurocode

2 [41], concrete starts to lose its compressive strength after being exposed to a temperature of 100°C. On the other hand, column S1_1L_40_ni_A strengthened with one layer of FRCM, failed after 144 minutes of fire exposure, which was more than double the time required to fail its unconfined counterpart. By that time, the temperature at the FRCM interface and the longitudinal reinforcement reached around 900 and 590°C, respectively, indicating that the FRCM has already lost its structural significance and the steel reinforcement has also lost more than 60% of its yield strength. The temperature measured at the core of the column S1_1L_40_ni_A was about 410°C.

Column S1_2L_40_ni_A, strengthened with 2 layers of FRCM, was able to resist the applied load for around 162 minutes prior to failure, which is not significantly better than the 144 minutes duration exhibited in column S1_1L_40_ni_A. The FRCM layer in column S1_2L_50_ni_A became structurally ineffective, which suggests the need of insulation for the FRCM-strengthened columns regardless of the number of the FRCM layers used. Nevertheless, there was clearly a direct relation between the number of FRCM Layers and the exposure duration under standard fire event.

The observed axial deformations of the columns were the result of both the sustained load and the thermal exposure. At the preload phase, the unstrengthened column S1_0L_40_ni_A had an axial deformation of around 0.6 mm whereas it had an axial deformation of 2 mm at failure. On the other hand, S1_1L_40_ni_A had an initial axial deformation of around 0.5 mm and an axial deformation of 7 mm at failure. S1_2L_40_ni_A experienced an initial deformation of 0.4 mm and a deformation of around 5 mm at failure.

The overall deformations decreased as the number of FRCM layers increased at every point in time due to the higher stiffness of the columns strengthened with PBO-FRCM layers. However, this was mainly observed after the point of failure of the unstrengthened column in the 3 preloading scenarios. For example, columns S1_0L_40_ni_A, S1_1L_40_ni_A, and S1_2L_40_ni_A had almost identical displacements until 65 minutes of fire exposure. After the 65-minute mark, the time at which S1_0L_40_ni_A experienced failure, the displacements started to diverge. At 100 minutes, they had displacements of 4, 3.2, and 2.2 mm, respectively. Similar observations can be made for the columns loaded at 60 and 75% of the control column capacity (938 and 1173 kN respectively) as shown in Figure 23-b and Figure 23-c, respectively.

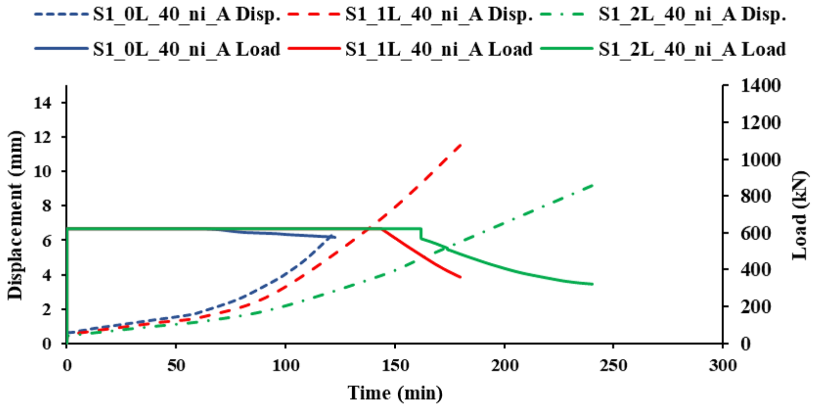

(a) 40% load

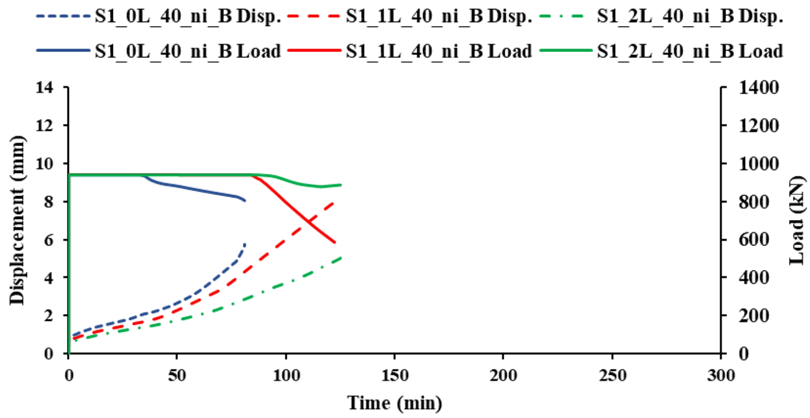

(b) 60% load

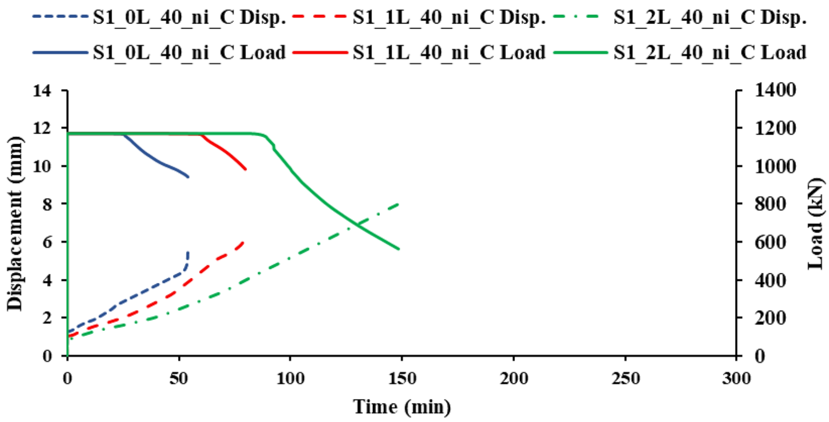

(c) 75% load

Figure 23: Series 1 load and displacement- time plots.

S1_1L_40_ni_B and S1_1L_40_ni_C resisted the applied loads for more than double the duration of their unstrengthened counterparts S1_0L_40_ni_B and S1_0L_40_ni_C respectively. In addition, the load resistance durations of S1_2L_40_ni_B and S1_2L_40_ni_C were slightly longer than those of their counterparts strengthened with 1 layer of PBO FRCM, S1_1L_40_ni_B and S1_1L_40_ni_C correspondingly. The relation between the number of layers and the overall deformation of the columns was also similar to that of the first 3 columns, S1_0L_40_ni_A, S1_1L_40_ni_A, and S1_2L_40_ni_A.

4.3.2.2. Effect of the applied axial load

To investigate the effect of the applied axial load, 40, 60, and 75% of the axial capacity of the tested columns were considered for the unstrengthened specimens, the specimens strengthened with 1 layer of FRCM, and the specimens strengthened with 2 layers of FRCM. Columns S2_0L_40_ni_A, S2_0L_40_ni_B, and S2_0L_40_ni_C, were axially loaded with 625, 938, and 1172 kN, respectively. Their load-time and deformation-time plots are shown in Figure 24-a. When loaded at 40% of its ultimate capacity, the unstrengthened column S2_0L_40_ni_A failed after around 65 minutes of fire exposure and the temperature in its longitudinal reinforcement and concrete core reached 335°C and 160°C, respectively, as previously mentioned. Columns S2_0L_40_ni_B and S2_0L_40_ni_C loaded at 60 and 75% of their ultimate capacity failed after 35 and 25 minutes, respectively. This finding shows that column S2_0L_40_ni_A (loaded at 40% of its capacity) could resist the applied load for almost double the duration of its counterpart S2_0L_40_ni_B (loaded at 60% of its capacity).

On the other hand, the difference between the time to failure of columns S2_0L_40_ni_B and S2_0L_40_ni_C was insignificant. The longitudinal bars of columns S2_0L_40_ni_B and S2_0L_40_ni_C reached temperatures of 190 and 130°C at failure, respectively. According to Eurocode 2 [41], the yield strength of the reinforcing bars was slightly affected by the fire exposure in both columns since the steel temperature exceeded 100°C. As for the concrete core temperatures, they reached 60°C and 35°C in both columns, respectively. Since the core temperatures did not reach 100°C, the concrete of both columns was not affected by the fire exposure. Another observation was the gradual load drop of column S2_0L_40_ni_A compared to the sharp drop in load in columns S2_0L_40_ni_B and S2_0L_40_ni_C, which suggested a more ductile behavior for the column S2_0L_40_ni_A (loaded with 40% of its ultimate capacity) compared to the ones loaded with 60 and 75% of their ultimate capacity. It can therefore be concluded that the higher the applied load during the fire exposure, the sharper the drop was in the load resistance.

The initial deformations of columns S2_0L_40_ni_A, S2_0L_40_ni_B, and S2_0L_40_ni_C were 0.6, 1, and 1.3 mm, respectively, in the preload phase. At failure, the columns recorded deformations of 2, 2.1, and 3.1 mm, respectively. Moreover, the overall recorded displacements were significantly larger in the columns loaded at higher percentages of their ultimate capacity at every point in time. For example, after 20 minutes of fire exposure, the displacements for S2_1L_40_ni_A, S2_1L_40_ni_B, and S2_1L_40_ni_C had displacements of 1, 1.6, and 2.4 mm respectively. For the second and third group of columns in this series strengthened with 1 layer (S2_1L_40_ni_A, S2_1L_40_ni_B, and S2_1L_40_ni_C) and 2 layers (S2_2L_40_ni_A, S2_2L_40_ni_B, and S2_2L_40_ni_C) of FRCM respectively, increasing the axial preload had a similar effect as shown in Figure 24-b and Figure 24-c. The higher the preload the earlier the columns reached failure and the less ductile behavior they displayed. Moreover, the columns loaded with higher preload values had higher displacement values at all points in time compared to the ones loaded with a smaller % of their ultimate capacity.

4.3.2.3. Effect of the concrete clear cover

To study the effect of the concrete clear cover on the behavior of the tested columns, 3 different concrete covers were investigated in this research namely, 40, 50, and 60 mm. The columns in Series 2, S2_1L_40_ni_B, S2_1L_40_ni_C, S2_2L_40_ni_B, and S2_1L_40_ni_C, with a 40 mm clear cover were loaded according to their ultimate capacity measured in ABAQUS. The same columns were modeled with 50 and 60 mm covers for comparison. As mentioned earlier, the columns in Series 3A had a 50 mm concrete clear cover whereas the columns in Series 3B had a concrete clear cover of 60 mm. The load-time and deformation-time plots for the unstrengthened columns with 40, 50, and 60 mm clear covers are shown in Figure 25 (loaded at 60% of their ultimate capacity) and Figure 26 (loaded at 75% of their ultimate capacity).

As mentioned earlier, the temperatures of the longitudinal reinforcement at failure measured in columns S2_0L_40_ni_B and S2_0L_40_ni_C were 190 and 130°C, respectively, indicating that the steel yield strength was slightly affected in both specimens. This finding shows that the 40 mm cover was able to maintain the temperature of the reinforcement below its critical range until failure as previously discussed. Columns S3A_0L_50_ni_B and S3A_0L_50_ni_C failed after approximately 85 and 55 minutes of fire exposure at which the temperature of the reinforcement was 340 and 220°C, respectively. These columns were able to maintain the applied load for more than double the time of their counterparts with a cover of 40 mm. However, since the steel reinforcement did not lose a significant percentage of its yield strength in columns S2_0L_40_ni_B and S2_0L_40_ni_C of Series 2 by the time of failure, the longer duration was probably due to the larger cover in addition to the steel insulation effect.

On the other hand, columns S3B_0L_60_ni_B and S3B_0L_60_ni_C with 60 mm covers failed after fire exposure of 100 and 80 minutes, respectively, indicating that those specimens resisted the applied load for approximately triple the durations of their corresponding columns S2_0L_40_ni_B and S2_0L_40_ni_C with a 40 mm concrete cover respectively. However, as mentioned earlier for columns S3A_0L_50_ni_B and S3A_0L_50_ni_C, the longer duration could be explained by the larger cover that protected the steel bars. The temperature of the steel level was 330 and 265°C at failure, respectively.

The initial displacements of columns S3A_0L_50_ni_B and S3A_0L_50_ni_C in the preload phase were 0.8 and 1 mm correspondingly. At failure, both columns had displacements of 4.3 and 4.1 mm, respectively. For specimens S3B_0L_60_ni_B and S3B_0L_60_ni_C, the displacements in the preload stage were 0.7 and 0.9 mm, respectively, and 3.5 and 4.2 mm at failure. The overall displacement values during the fire exposure duration were generally lower for the columns with a larger concrete cover.

Similar observations were made for the columns of Series 2, 3A, and 3B strengthened with 1 and 2 layers of FRCM. Their load-time and displacement-time plots are also shown in Figures 25 and 26. Increasing the concrete cover led to longer exposure durations. Moreover, increasing the concrete cover led to lower overall displacements during the fire exposure.

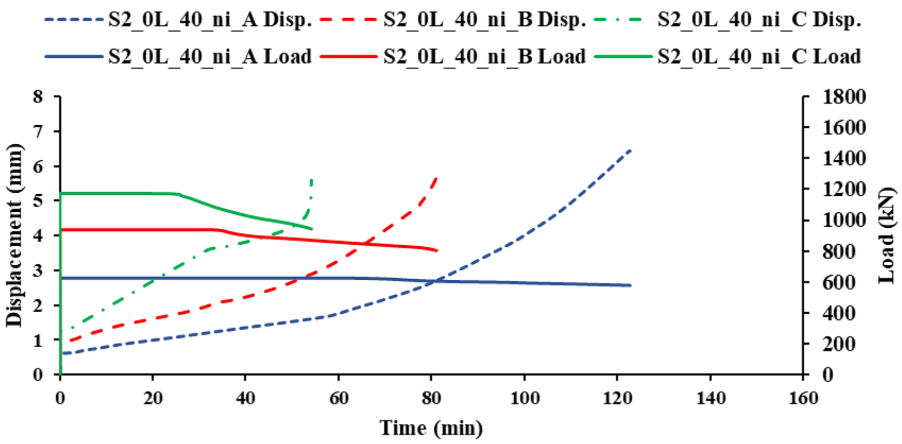

(a) Unstrengthened

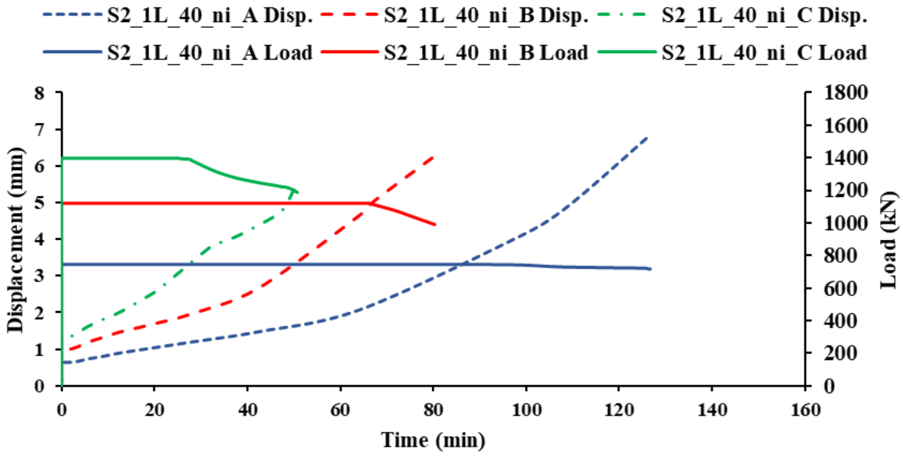

(b) 1 layer strengthened

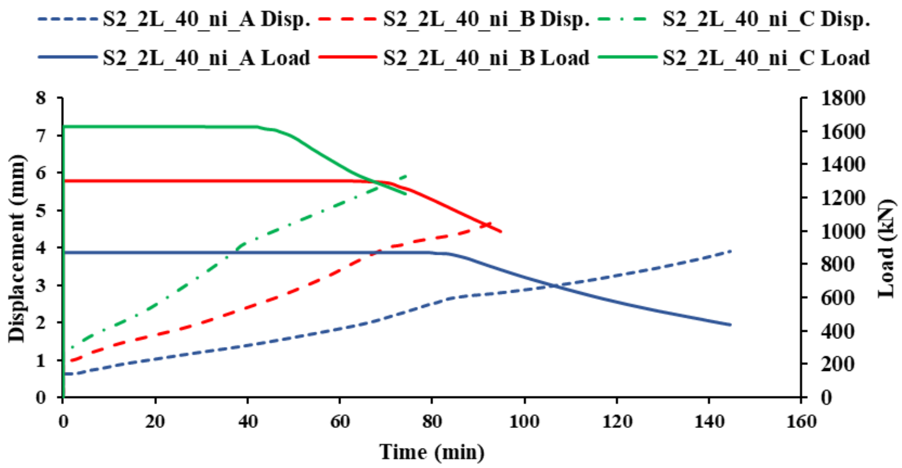

(c) 2 layer strengthened

Figure 24: Series 2 load and displacement- time plots.

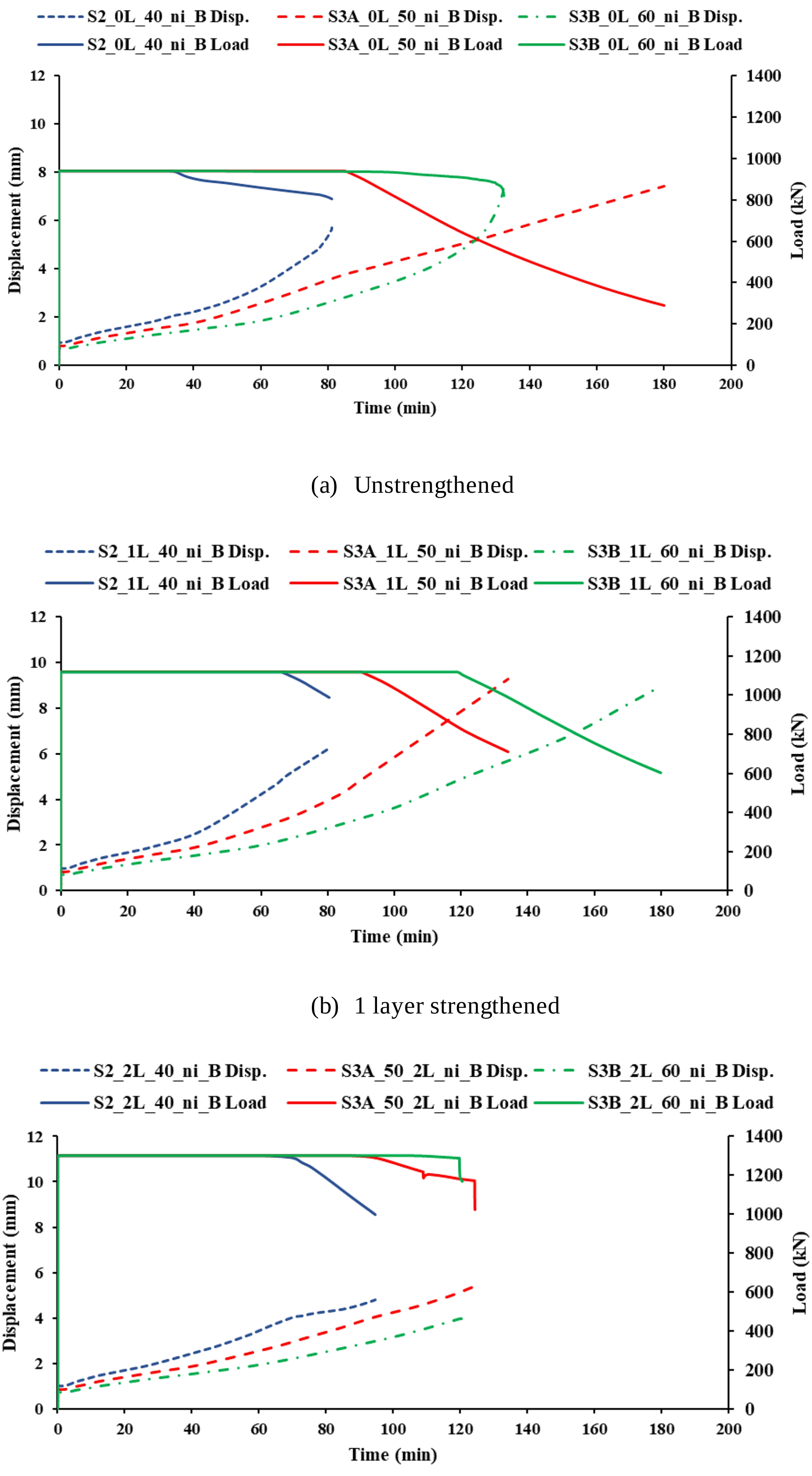

(a) Unstrengthened

(b) 1 layer strengthened

(c) 2 layer strengthened

Figure 25: Series 3A and 3B vs. Series 2 load and displacement- time plots for 60% load.

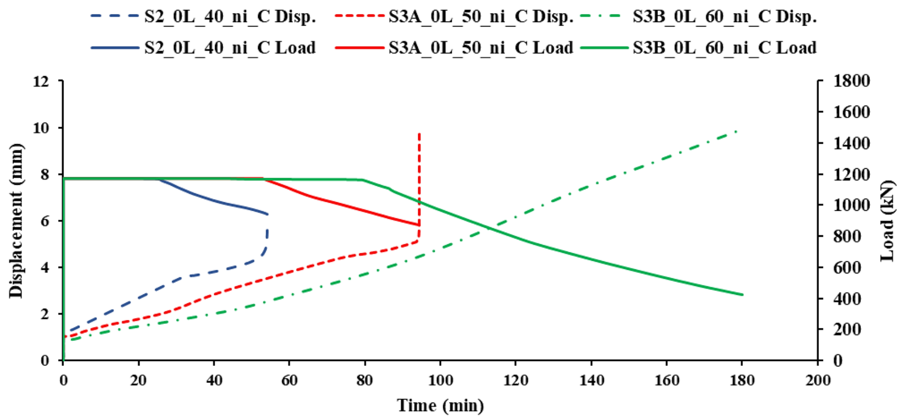

(a) Unstrengthened

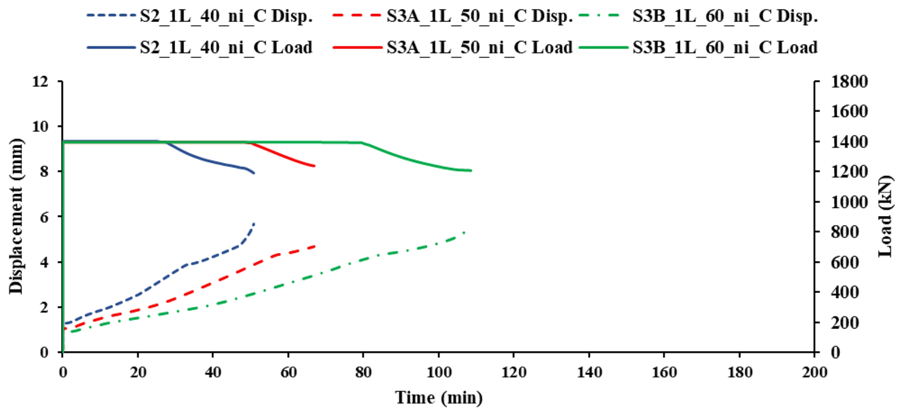

(b) 1 layer strengthened

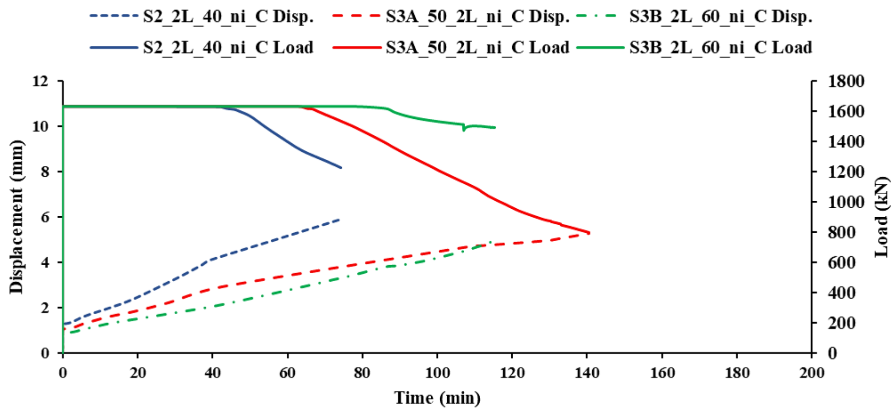

(c) 2 layer strengthened

Figure 26: Series 3A and 3B vs. Series 2 load and displacement- time plots for 75% load.

4.3.2.4. Effect of insulation

As previously mentioned in the discussion of specimens of Series 1, the replacement of organic based matrices with cement-based ones might not be sufficient enough to achieve the ultimate fire resistance of columns strengthened with externally bonded composite materials. Therefore, it is important to investigate the performance of FRCM-strengthened columns that are fireproofed with insulation material. The columns of the series 4 correspond to those of Series 2 with a 30 mm layer of insulation or fireproof material.

As discussed earlier, the insulation considerably reduced the temperatures throughout the cross sections of the columns. Figure 27 (40% load), Figure 28 (60% load), and Figure 29 (75% load) show the load-time and displacement-time curves for the unstrengthened columns of Series 4 and Series 2 for comparison. Since the insulation was successful in lowering the internal temperatures of the concrete, the load resistance durations of the insulated columns were significantly longer than their uninsulated counterparts. S4_0L_40_i_A, S4_0L_40_i_B, and S4_0L_40_i_C resisted the applied loads for 145, 125, and 100 minutes, which proved the effectiveness of the insulation in delaying the failure time of the columns compared to their uninsulated counterparts in Series 2. For example, the temperature at the level of the concrete surface in column S2_0L_40_ni_A was 720°C at failure (after 65 minutes) compared to 440°C in column S4_0L_40_i_A (at failure after 145 minutes).

Similar response was observed for the columns of Series 2 and 4 strengthened with 1 and 2 layers of PBO FRCM layers as shown in Figures 27, 28, and 29. The strengthened columns with a fire protection layer resisted the applied load for a significantly longer duration compared to their corresponding uninsulated columns. For example, the temperature at the level of FRCM in column S2_1L_40_ni_B was 715°C after a duration of around 65 minutes after which failure occurred. However, the temperature in column S4_1L_40_i_B at the same location was around 580°C after 215 minutes before the column was unable to further resist the applied load.

An additional observation was the ability of the strengthened columns loaded at 40% of their axial capacity to resist the load for the entire duration of the test (300 minutes) without failure, namely columns S4_1L_40_i_A and S4_2L_40_i_A. The insulation was also effective in reducing the overall displacements of the columns. The displacement measured in the columns of Series 4 were significantly lower than the displacements of their corresponding uninsulated columns. For example, in Figure 27, S2_1L_40_ni_A had a displacement of around 1mm after 1 hour of fire exposure

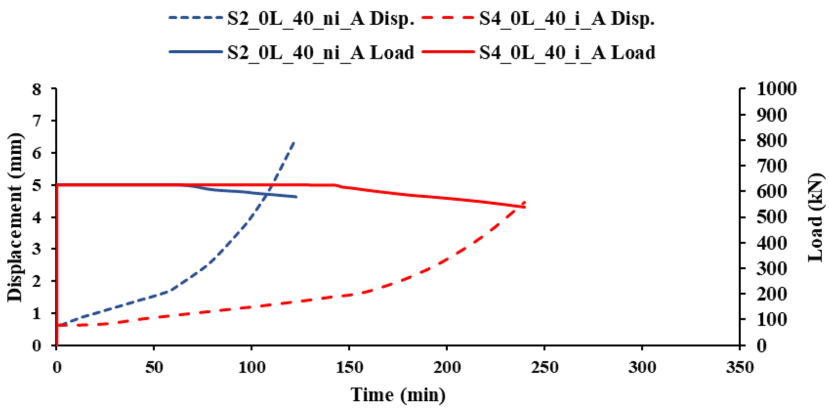

(a) Unstrengthened

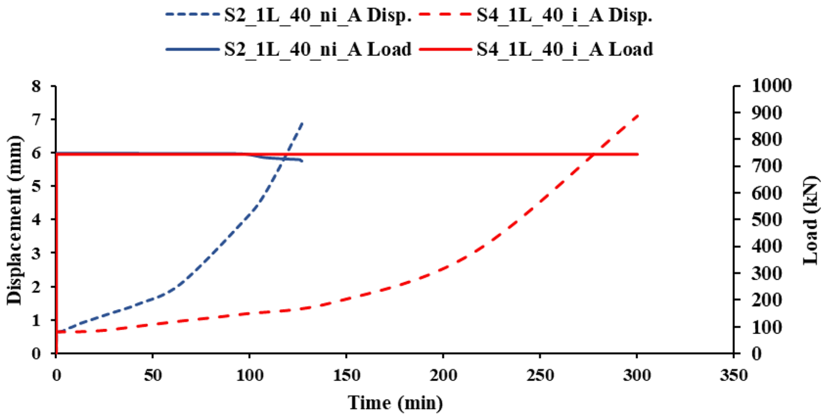

(b) 1 layer strengthened

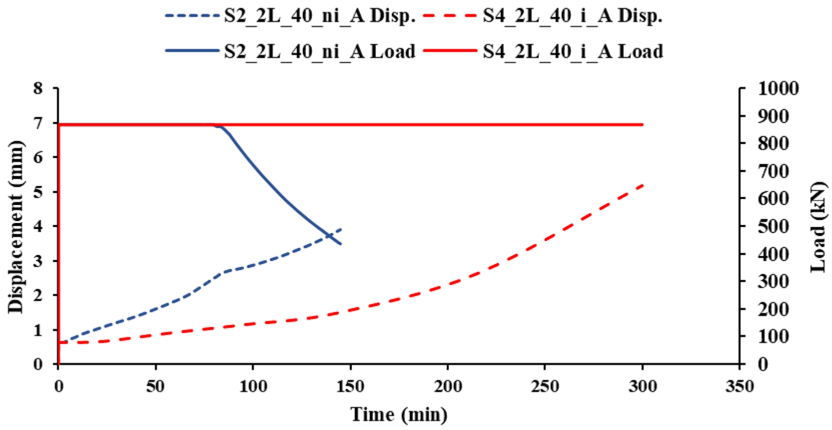

(c) 2 layer strengthened

Figure 27: Series 4 vs. Series 2 load and displacement- time plots for 40% load.

compared to S4_1L_40_i_A which had a displacement of 1.8 mm. The effect of the insulation in reducing the overall displacements was more pronounced for the columns loaded at 75% of their axial capacity.

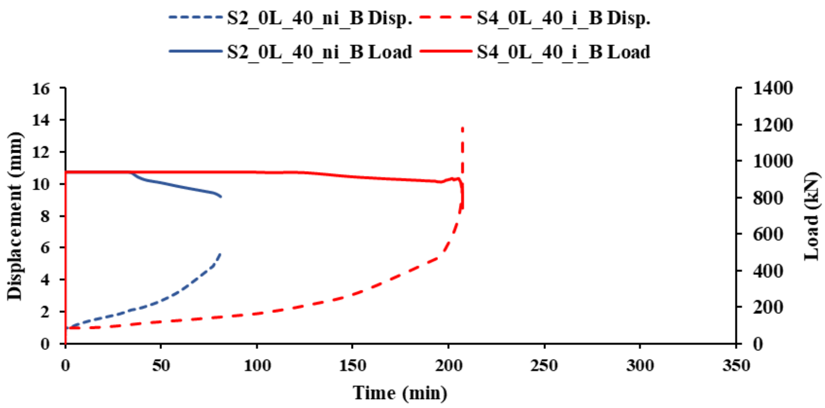

(a) Unstrengthened

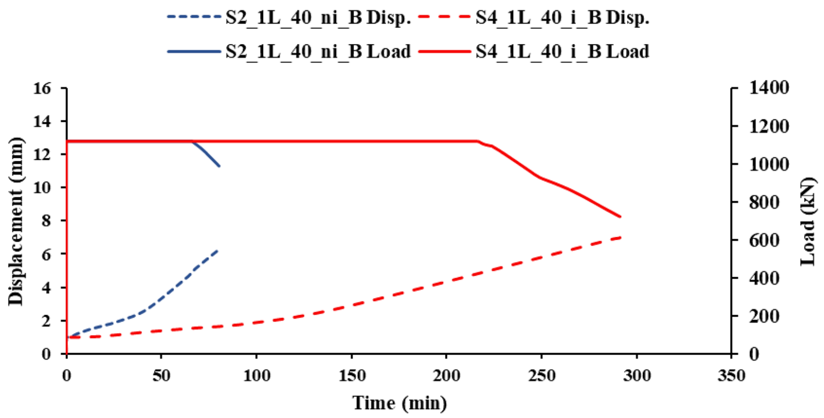

(b) 1 layer strengthened

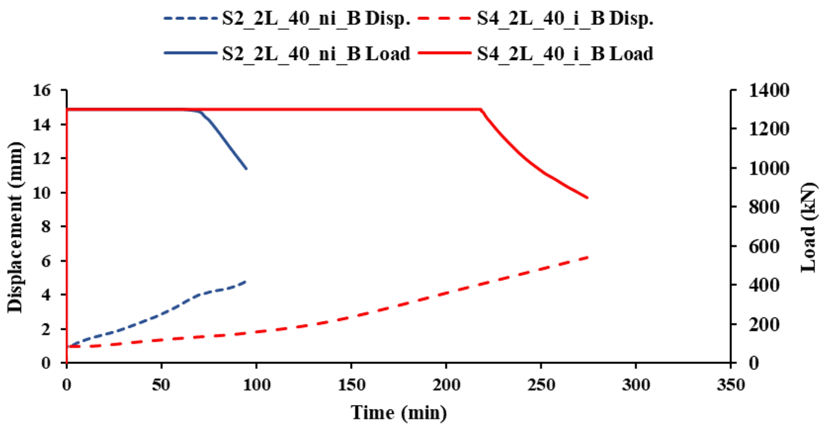

(c) 2 layer strengthened

Figure 28: Series 4 vs. Series 2 load and displacement- time plots for 60% load.

For example, the same columns loaded at 75% of their axial capacity, S4_1L_40_i_C and S2_1L_40_ni_C, had displacements of 1.6 and 3.4 mm (more than double) after around 30 minutes of fire exposure as shown in Figure 29.

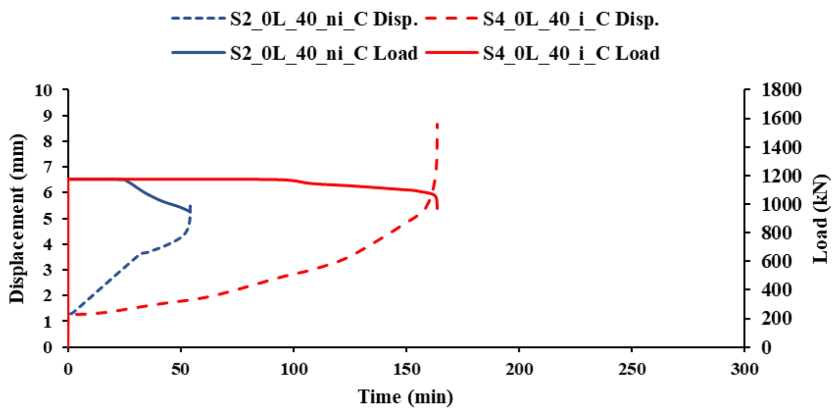

(a) Unstrengthened

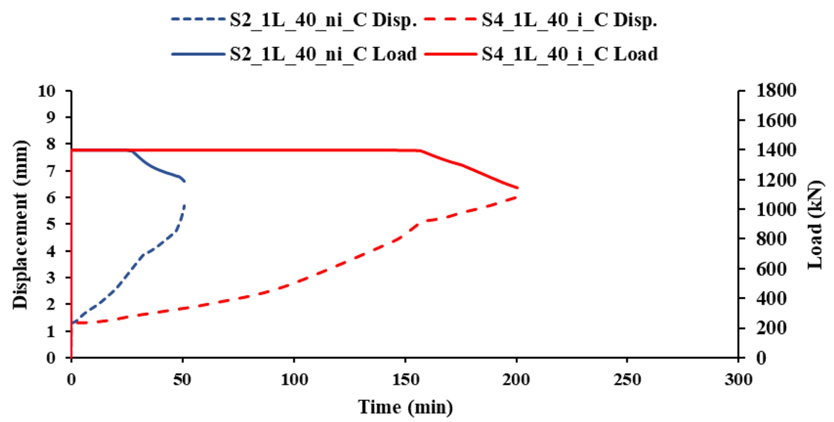

(b) 1 layer strengthened

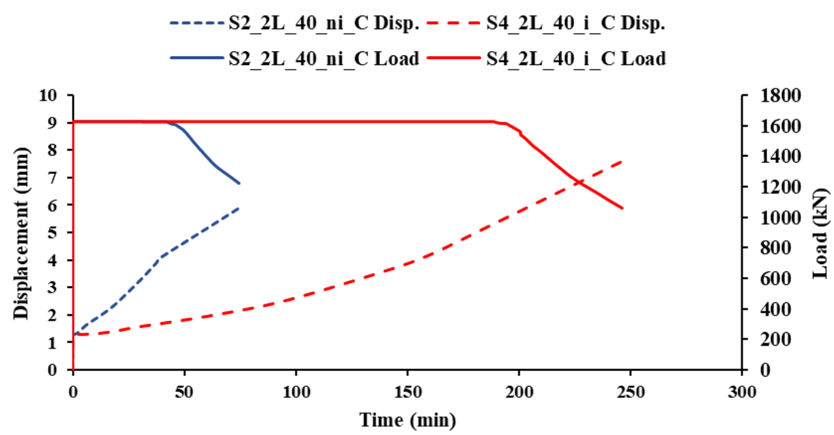

(c) 2 layer strengthened

Figure 29: Series 4 vs. Series 2 load and displacement- time plots for 75% load.

Table 7 summarizes the load resistance durations of all the modeled specimens in Series 1, 2, 3A, 3B, and 4.

4.3.3. Mises stress contours

In this section, the stress distribution of the columns is discussed and selected stress contours are shown. A general observation for all the columns was the weakening in the concrete that was close to the fire exposure compared to the regions closer to the core. The concrete core is expected to resist the applied load throughout the fire exposure as the fire is directly affecting the regions of the column closer to the surface. Therefore, most of the resistance is achieved by the concrete core.

Figure 30 shows the concrete and steel stress contours for S1_0L_40_ni_B, S1_1L_40_ni_B, and S1_2L_40_ni_B. The core stresses for all the columns exceeded 30 MPa (the compressive strength of concrete in the room temperature), which suggested the crushing of concrete. On the other hand, the stresses at failure in the reinforcing bars and ties decreased with the addition of FRCM layers as shown in Figure 30. The stresses in the longitudinal reinforcement decreased by an average of 39 and 45% when 1 and 2 layers of FRCM were added. For the ties, an average decrease of 19 and 25% was observed correspondingly. This could be explained by the redistribution of stresses in the cross section with the presence of the FRCM strengthening.

However, there was an inconsistent trend in terms of yielding of the steel bars. Some columns showed yielding in both their reinforcement, some only in the bars, while others showed no yielding at all.

Figure 31 shows the stress contours for the FRCM, concrete, and steel at failure for S2_1L_40_ni_A, S2_1L_40_ni_B, and S2_1L_40_ni_C. The overall stress values were higher in the columns that were loaded with a higher percentage of their ultimate capacity. For instance, increasing the load from 40 to 60% of the capacity led to an average increase of 13% in the concrete core stresses. On the other hand, a load of 75% of the column capacity led to an average increase of around 26%. Moreover, the core stresses for all 3 load ratios exceeded 30 MPa, the compressive strength of concrete at room temperature, which could be explained by the weakening of the regions in the cross section closer to the outer surface as mentioned earlier. This suggested that concrete crushed in the core for the 3 preloading scenarios in which the column strengthened with 1 layer of FRCM in Series 2 was loaded at 40, 60, and 75% of its ultimate capacity.

Table 7: Load Resistance Durations

Series	Specimen ID	Load Resistance Duration (min)
1	S1_0L_40_ni_A	65
	S1_1L_40_ni_A	144
	S1_2L_40_ni_A	162
	S1_0L_40_ni_B	35
	S1_1L_40_ni_B	84
	S1_2L_40_ni_B	95
	S1_0L_40_ni_C	25
	S1_1L_40_ni_C	60
	S1_2L_40_ni_C	88
2	S2_0L_40_ni_A*	65
	S2_0L_40_ni_B*	35
	S2_0L_40_ni_C*	25
	S2_1L_40_ni_A	100
	S2_1L_40_ni_B	65
	S2_1L_40_ni_C	27
	S2_2L_40_ni_A	84
	S2_2L_40_ni_B	70
	S2_2L_40_ni_C	43
3A	S3A_0L_50_ni_B	85
	S3A_0L_50_ni_C	55
	S3A_1L_50_ni_B	90
	S3A_1L_50_ni_C	50
	S3A_2L_50_ni_B	95
	S3A_2L_50_ni_C	63
3B	S3B_0L_60_ni_B	100
	S3B_0L_60_ni_C	80
	S3B_1L_60_ni_B	120
	S3B_1L_60_ni_C	80
	S3B_2L_60_ni_B	120
	S3B_2L_60_ni_C	86
4	S4_0L_40_i_A	145
	S4_0L_40_i_B	125
	S4_0L_40_i_C	100
	S4_1L_40_i_A	-
	S4_1L_40_i_B	215
	S4_1L_40_i_C	157
	S4_2L_40_i_A	-
	S4_2L_40_i_B	219
	S4_2L_40_i_C	195

*Indicates specimens repeated from Series 1

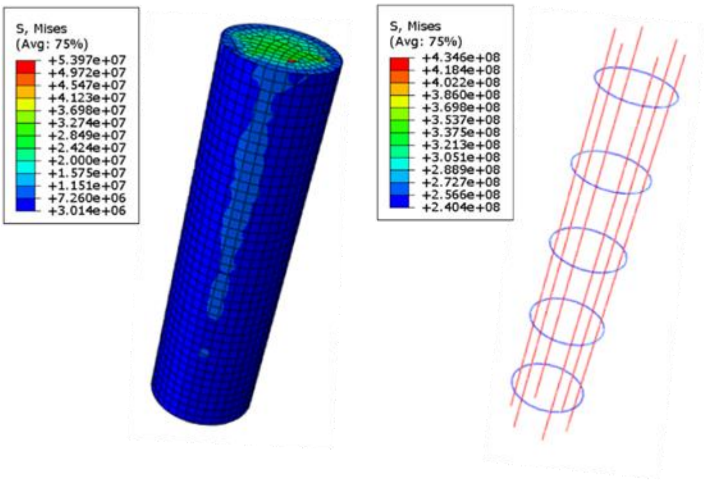

(a) S1_0L_40_ni_B

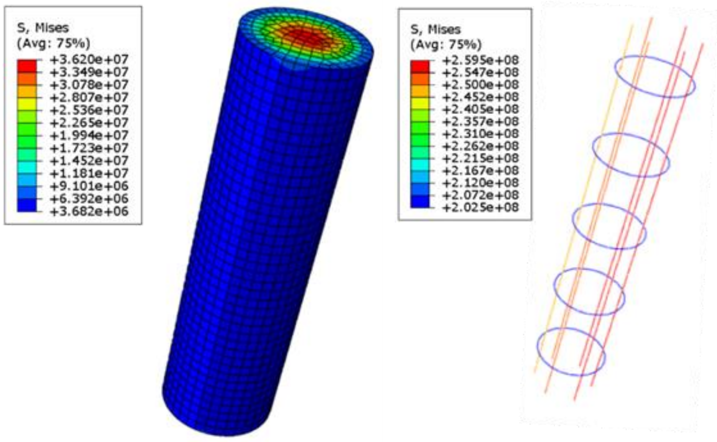

(b) S1_1L_40_ni_B

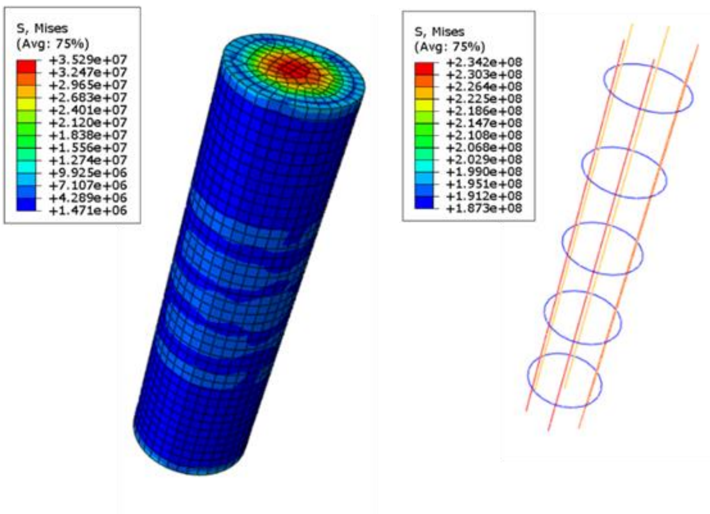

(c) S1_2L_40_ni_B

Figure 30: Concrete and steel stress contours.

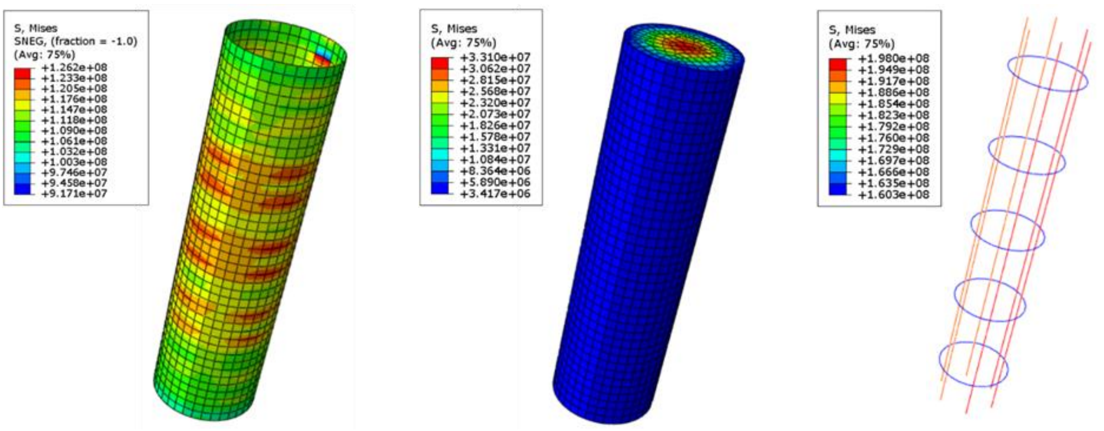

(a) S2_1L_40_ni_A

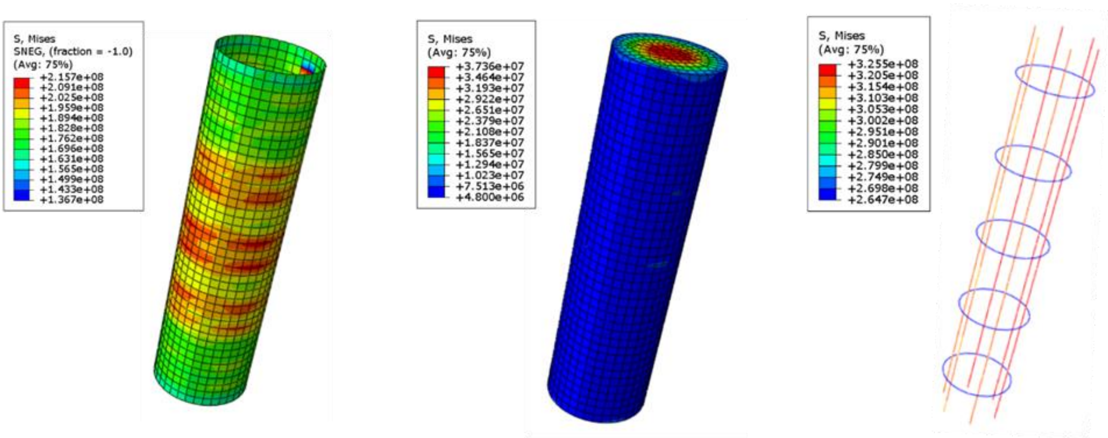

(b) S2_1L_40_ni_B

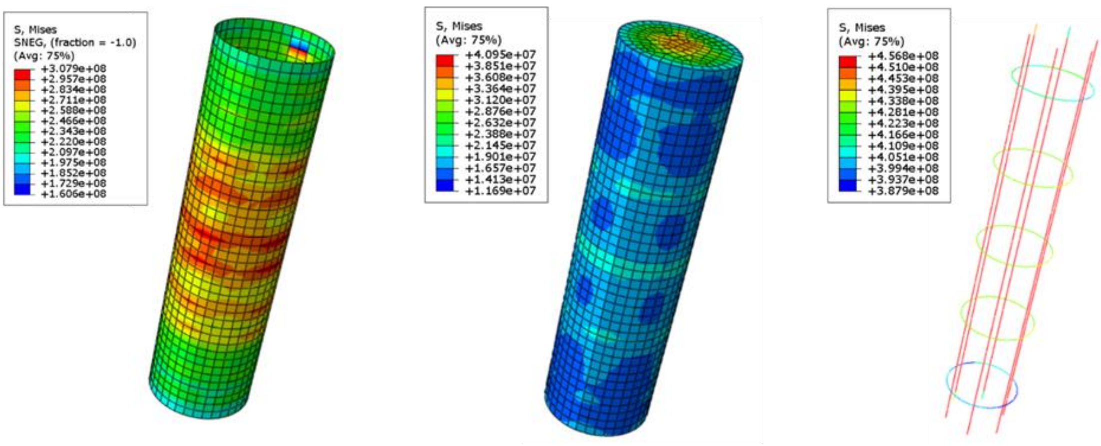

(c) S2_1L_40_ni_C

Figure 31: FRCM, concrete, and steel stress contours.

Steel yielding occurred in almost all the columns of Series 2. For example, the steel stress contours for the 1 layer strengthened columns indicated yielding according to the yield stress relations with temperature for steel provided by Eurocode 2 [41] for all considered preloading scenarios. There was an inconsistent trend regarding the yielding of steel. In some columns, only the longitudinal reinforcement yielded while in other cases, yielding of both the longitudinal reinforcement and ties occurred.

For the FRCM layers, the obtained stress contours indicated their rupture in several columns. Figure 31 shows that the stresses exceeded the tensile strength of the FRCM corresponding to the temperature reached at failure for S2_1L_40_ni_A and S2_1L_40_ni_B suggesting their rupture. Since a perfect bond was assumed between the FRCM and the concrete substrate, debonding failure was not accounted for, however, this scenario could possibly occur. The stresses for the 75% preloading scenario indicated that the FRCM tensile strength at failure was not exceeded in column S2_1L_40_ni_C.

Chapter 5. Experiments on PBO FRCM- Confined Cylinders

Experimental tests were performed on PBO FRCM- confined cylinders heated to several target temperatures and then loaded in axial compression until failure. The aim of the performed experiments was to gain a better understanding of the performance and confinement effect of the PBO FRCM systems under elevated temperatures (up to 800°C). Details about the specimens and the performed tests are presented and explained in this chapter.

5.1. Experimental Program

The details of the experimental program, which was divided into 3 groups are presented in Table 8, Table 9, and Table 10. The investigation was carried out on a total of 34 specimens including cylinders of normal compressive strength concrete (30 MPa), medium strength (45 MPa), and high strength (70 MPa) confined with 1 and 2 layers in addition to the control unconfined specimens. All the tested cylinders had a length of 300 mm and a diameter of 150 mm (before confining).

5.2. Specimen Preparation

The cylindrical specimens were cast using 3 concrete batches of 30, 45, and 70 MPa. The specimens were left in curing tanks for 28 days prior to confinement.

Table 8: Group 1

Specimen ID	Concrete Strength (MPa)	Number of Layers	Target Temperature (°C)
RT_0L_30	30	0	-
100_0L_30	30	0	100
400_0L_30	30	0	400
800_0L_30	30	0	800
RT_1L_30	30	1	-
100_1L_30	30	1	100
400_1L_30	30	1	400
800_1L_30	30	1	800
RT_2L_30	30	2	-
100_2L_30	30	2	100
400_2L_30	30	2	400
800_2L_30	30	2	800

Table 9: Group 2

Specimen ID	Concrete Strength (MPa)	Number of Layers	Target Temperature (°C)
RT_0L_45	45	0	-
100_0L_45	45	0	100
400_0L_45	45	0	400
800_0L_45	45	0	800
RT_1L_45	45	1	-
100_1L_45	45	1	100
400_1L_45	45	1	400
800_1L_45	45	1	800
RT_2L_45	45	2	-
400_2L_45	45	2	400

Table 10: Group 3

Specimen ID	Concrete Strength (MPa)	Number of Layers	Target Temperature (°C)
RT_0L_70	70	0	-
100_0L_70	70	0	100
400_0L_70	70	0	400
800_0L_70	70	0	800
RT_1L_70	70	1	-
100_1L_70	70	1	100
400_1L_70	70	1	400
800_1L_70	70	1	800
RT_2L_70	70	2	-
100_2L_70	70	2	100
400_2L_70	70	2	400
800_2L_70	70	2	800

The properties of the PBO fabric used are presented in Table 11. A binding cementitious material with a compressive strength of 40 MPa was used.

Table 11: PBO Textile Properties

Material	Ruregold PBO FRCM
Nominal Thickness (mm)	0.05
Young's Modulus, E_f (GPa)	270
Tensile Strength, f_{fu}, (MPa)	5800

The textile was cut into sheets of 300 mm width (total height of the cylinder) and 471 mm length (equivalent to the length of the cylinder's circumference) plus 100 mm to account for the overlap length. Prior to confinement, an electric grinder was used to roughen the outer surface of the cylinder to ensure good bonding between the cementitious material and the concrete substrate. An initial mortar layer was applied with an approximate thickness of 3 mm.

To ensure the desired thickness, the cementitious layer was placed in 3 mm thick acrylic frames before wrapping as shown in Figure 32. The cement was smoothened with a metal rod to ensure an overall uniform thickness. After demoulding the cement layer, it was applied to the cylinder using the rolling technique shown in Figure 33.

Figure 32: Molding and demolding of the first cementitious layer.

(a) (b)

Figure 33: Cylinder (a) before and (b) after first cement layer application.

After applying the cement layer, a layer of PBO fabric was applied as shown in Figure 34. The fabric was slightly pressed and impregnated in the mortar before the second mortar layer and fabric were applied using the same procedure as shown in Figure 34 for cylinders confined with 1 and 2 FRCM layers. The cylinders were then left to cure by wrapping a wet burlap around them until the day of testing.

Figure 34: (a) PBO sheet application, (b) 1 layer confined cylinder, and (c) 2 layer confined cylinder.

5.3. Thermal Exposure

A furnace with a heating capacity of 1000°C was used to heat the specimens. The heating was done for an average of 5 specimens at a time as shown in Figure 35.

Figure 35: Cylinders prior to heating.

All cylinders were heated to steady-state temperatures up to 800°C at a heating rate of 10°C/min. Once the target temperature was reached, they were kept in the furnace at the target temperature for 1 hour after which they were removed from the oven and left to cool to room temperature conditions. Figure 36 shows the temperature vs. time curves that were followed.

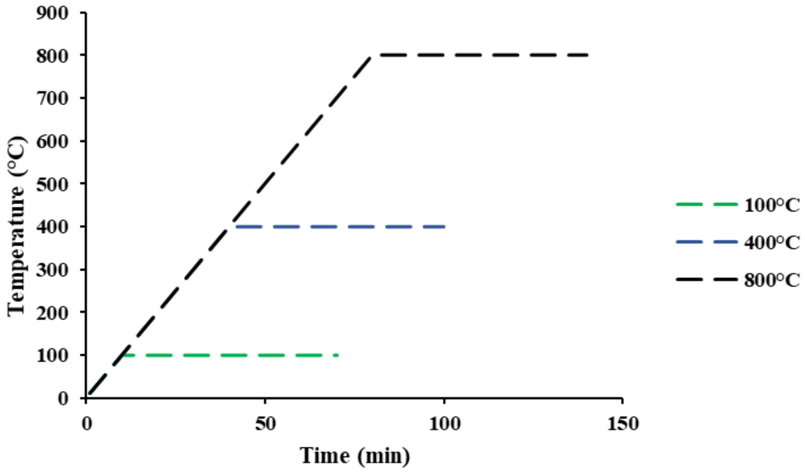

Figure 36: Individual temperature-time curves used in the experiments.

5.4. Compression Tests

After all specimens were cooled to ambient temperature, they were tested in axial compression until failure. A 3000 kN SANS compression machine was used to load the cylinders according to ASTM C39 standards [51]. Load–time graphs were obtained for each specimen. The standard cap diameter for the machine was 150 mm, which didn't fit the in the confined cylinders due to their larger diameters. Therefore, to prevent premature failure during testing, 2 layers of CFRP strips were applied on the top and bottom of the cylinders with an average height of 30 mm, as shown in Figure 37.

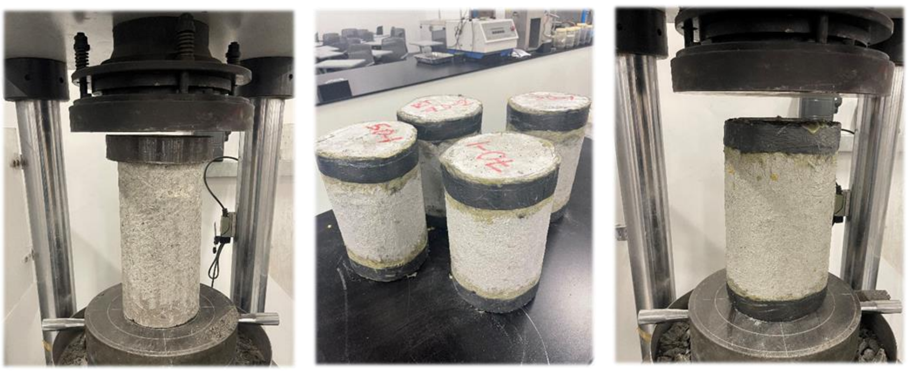

Figure 37: Unconfined and confined cylinder test setup.

5.5. Results and Discussion

The results of the performed tests are presented in Table 12. The observed failure modes and the effect of concrete strength, number of layers, and temperature exposure on the experimental results are discussed in the following sections.

Table 12: Cylinder Compression Test Results

Group	Specimen ID	Ultimate Load (kN)	Compressive Strength (MPa)
1	RT_0L_30	527.7	29.9
	100_0L_30	613.1	34.7
	400_0L_30	461.0	26.1
	800_0L_30	97.7	5.5
	RT_1L_30	729.4	41.3
	100_1L_30	786.7	44.5
	400_1L_30	518.2	29.3
	800_1L_30	282.5	16.0
	RT_2L_30	935.0	52.9
	100_2L_30	750.0	42.5
	400_2L_30	859.6	48.7
	800_2L_30	368.0	20.8
2	RT_0L_45	743.0	42.1
	100_0L_45	877.1	49.7
	400_0L_45	676.3	38.3
	800_0L_45	344.6	19.5
	RT_1L_45	838.1	47.5
	100_1L_45	906.8	51.3
	400_1L_45	903.0	51.1
	800_1L_45	587.3	33.3
	RT_2L_45	938.9	53.2
	400_2L_45	983.7	55.7
3	RT_0L_70	1218.3	69.0
	100_0L_70	1430.0	81.0
	400_0L_70	1306.9	74.0
	800_0L_70	848.6	48.0
	RT_1L_70	1406.8	79.6
	100_1L_70	1692.8	95.8
	400_1L_70	1312.8	74.3
	800_1L_70	1024.2	58.0
	RT_2L_70	1455.0	82.4
	100_2L_70	1434.7	81.2
	400_2L_70	1511.8	85.6
	800_2L_70	1026.8	58.1

5.5.1. Failure modes

Figure 38, Figure 39, and Figure 40 show the failure modes of selected specimens from Group 1, Group 2, and Group 3, respectively.

RT_1L_30

100_2L_30

400_2L_30

800_1L_30

Figure 38: Group 1 failure modes.

It is important to note that the specimens were prepared using the hand layup method, which cannot ensure perfect alignment of the fibers, uniform cement thickness, proper impregnation of the fibers, and the exact overlap length for all the specimens. Such imperfections and nonuniformity in the FRCM systems might explain the discrepancy in some of the test results, as detailed later. It was also observed that the FRP strips used instead of the machine cap were not perfectly aligned and bonded to the substrate.


RT_2L_45 100_1L_45


400_1L_45 800_1L_45

Figure 39: Group 2 failure modes.

For all the tested cylinders, a gradual formation of cracks in the outer mortar layer was observed. In most of the cylinders, failure occurred due to the separation in the fabric-matrix interface. In a few specimens, the rupture or debonding of the FRP strips was observed during testing, which has led to a premature failure in 100_2L_30 and 100_1L_45.

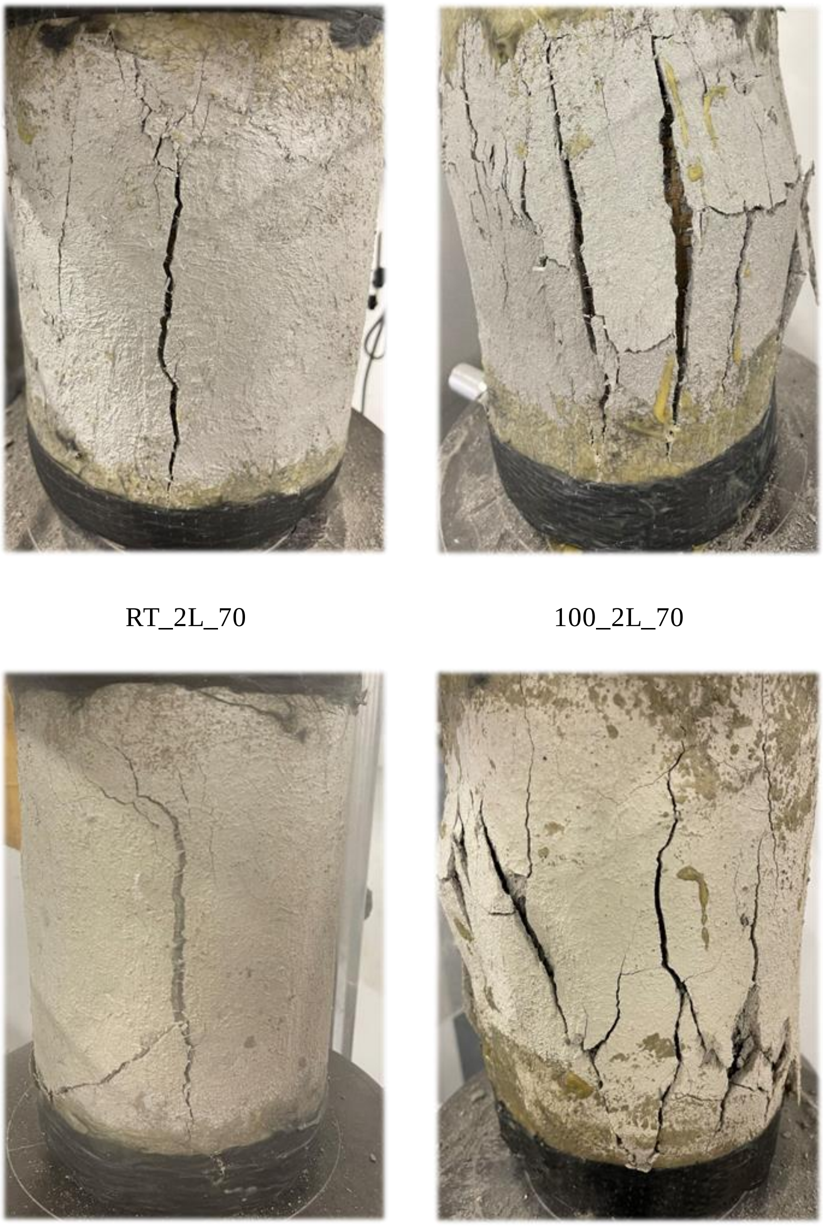

RT_2L_70 100_2L_70

400_1L_70 800_2L_70

Figure 40: Group 3 failure modes.

5.5.2. Effect of the concrete strength and the number of FRCM layers

The variation of the compressive strength of the control and the confined cylinders are presented in Figure 41. As indicated from the obtained results, the effect of FRCM confinement on the compressive strength was more pronounced in the specimens of group 1 with f'_c of 30 MPa.

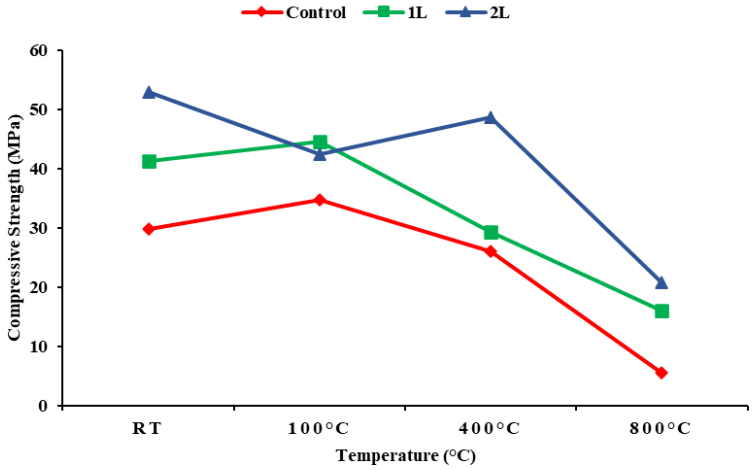

(a) Group 1

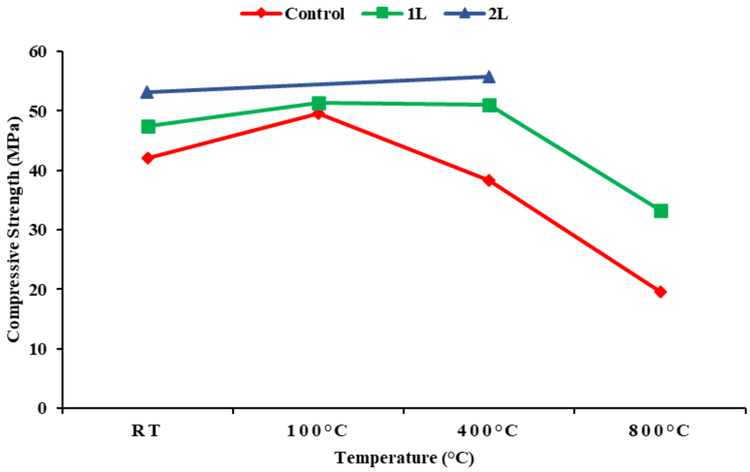

(b) Group 2

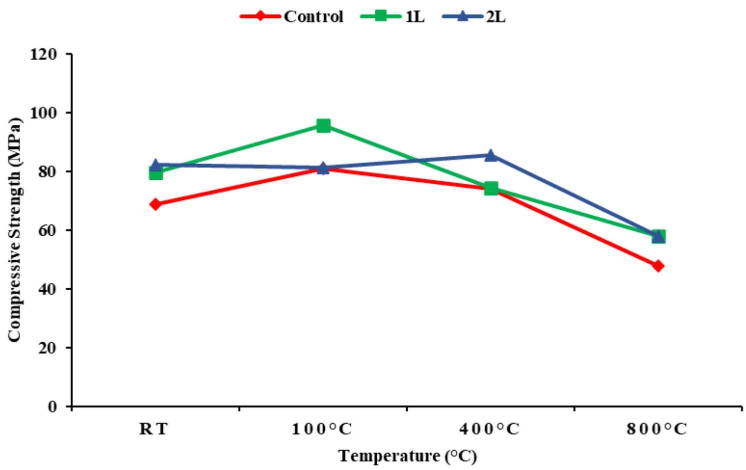

(c) Group 3

Figure 41: Compressive strength vs. temperature.

At room temperature, confining the tested specimens with 1 and 2 layers of FRCM increased the compressive strength 38 and 77% respectively relative to the control cylinder (RT_0L_30) in group 1 compared to an increase of 13 and 26% in specimens of group 2, and 16 and 19% in specimens of group 3. Given the relatively high concrete strengths in specimens of groups 2 and 3, it was expected to observe a less significant increase in strength when adding FRCM confinement.

Despite some discrepancies, similar conclusions can be drawn for specimens of all groups at all temperature exposures. Confining the specimens with one and two layers impeded the effect of temperature on the compressive strength of the tested specimens as detailed below.

It is important to note that several reasons have led to the discrepancies shown in Figure 41. For instance, specimens 100_2L_30 of group 1 and 100_2L_70 of group 3, which were confined with 2 layers of FRCM and heated to 100°C, showed compressive strengths lower than their counterparts 100_1L_30 and 100_1L_70, respectively, which were confined with only one layer. This finding was attributed to the premature rupture and debonding of the lower FRP strip as observed during testing and shown in Figure 38 for specimen 100_2L_30.

5.5.3. Effect of the elevated temperature

The effect of the exposure temperature on the compressive strength of all the tested cylinders is shown in Table 13.

Table 13: % Decrease/Increase in Compressive Strength

Group	No. of Layers	% Decrease/Increase in Compressive Strength			
		RT	100°C	400°C	800°C
1	0	-	+16%	-13%	-82%
	1	-	+8%	-29%	-61%
	2	-	-20%	-8%	-61%
2	0	-	+18%	-9%	-54%
	1	-	+8%	+8%	-30%
	2	-	-	+5%	-
3	0	-	+17%	+7%	-30%
	1	-	+20%	-7%	-27%
	2	-	-1%	+4%	-29%

5.5.3.1. Control unconfined cylinders

For the control unconfined cylinders, a minor increase in strength (an average of 17%) was observed when the specimens were heated to 100°C. This trend was true for specimens of all concrete strengths (groups 1, 2, and 3). This finding agreed well with the provisions of Eurocode 2 that states that the compressive strength of concrete undergoes a negligible change in strength when it is heated to 100°C [41]. Minor increase in the compressive strength of normal concrete has been reported by Kodur [17] while other studies showed that heating the concrete to 100°C has caused a slight drop in its compressive strength [15], [52], [53]. In the current study, the increase in strength was observed in specimens of all groups and was almost consistent. This finding may be attributed to the prolonged curing of concrete, which simulated steam curing or hot air curing, in which concrete is exposed to hot water vapor (up to 100°C) to accelerate its strength development [54], despite the fact that the cylinders were heated after more than 90 days of their casting day. On the other hand, heating the control cylinders to 400°C slightly affected their compressive strength, which agreed well with the results reported by Kodur [17]. The highest loss in strength of the tested specimens was 13% and was encountered in specimen 400_0L_30 of group 1. Specimen 400_0L_45 of group 2 lost around 9% of its capacity; however, specimen 400_0L_70 experienced a minor increase in strength of 7%.

At 800°C, all control specimens suffered from a significant decrease in their compressive strength. The highest decrease in strength, 82%, corresponded to specimen 800_0L_30 of group 1, which agreed well with the test results of Chan et al. [55]. Specimens 800_0L_45 and 800_0L_30 of groups 2 and 3 lost 54 and 30% of their capacity, respectively.

5.5.3.2. Confined cylinders

The elevated temperature had a similar effect on the specimens confined with 1 layer of FRCM compared to the unconfined specimens. A minor increase in strength was also observed at 100°C. At 400°C, the highest decrease in strength was about 29%, which corresponded also to the specimen 400_1L_30 in Series 1. Specimens heated at 800°C also experienced significant decreases in their strength.

The residual strengths of the cylinders confined with 2 layers of FRCM and heated at 100°C indicated that the elevated temperatures did not have the same effect on their strength as on the unconfined cylinders and the cylinders confined with 1 layer of FRCM. Heating the cylinders to 100°C resulted in a 20% decrease in capacity for specimens 100_2L_30 in group 1 and almost no decrease in capacity for specimens 100_2L_70 in group 3. This suggested that the FRCM might have impeded the effect of the elevated temperature, which resulted in a different behavior. Up to 400°C, the temperature exposure did not have a significant effect on the residual capacity as observed for the unconfined specimens and the specimens confined with 1 layer of FRCM. The cylinders heated to 800°C also experienced significant drops in capacity, indicating that at high temperatures, the number of confinement layers did not affect the decrease in strength.

Chapter 6. Conclusions

The present study aimed at investigating the fire performance of PBO FRCM-strengthened RC columns. Finite Element models were developed using ABAQUS to study the fire performance of FRCM-strengthened columns, while examining the influence of parameters such as concrete clear cover, number of FRCM layers, presence of a 30 mm thick insulation layer, and axial preloading. Additionally, experiments were performed on PBO FRCM-confined concrete cylinders to investigate the effect of concrete strength, number of FRCM layers, and target temperature on compressive strength. The following conclusions were drawn from the FE Analysis:

1. The proposed FE model successfully predicted temperatures at different cross-section levels for insulated, uninsulated, FRP- strengthened, FRCM-strengthened, and unstrengthened RC columns.
2. Increasing the concrete cover resulted in lower temperatures at the reinforcement level at each time increment. After 1 hour of fire exposure, the steel reinforcement temperature was 14% and 27% lower in columns with concrete clear covers of 50 and 60 mm, respectively, compared to columns with 40 mm cover.
3. The inclusion of a 30 mm insulation layer significantly reduced temperatures across the cross-section. In Series 4 columns, the temperature drop after 1 hour of fire exposure was approximately 70% at the FRCM surface for the insulated column strengthened with 1 layer of FRCM, compared to the corresponding specimen in Series 2.
4. Strengthening Series 1 specimens with 1 and 2 layers of FRCM effectively increased the duration of load resistance. Adding 1 layer of FRCM more than doubled the duration compared to its unstrengthened counterpart, while adding 2 layers did not significantly further increase the duration since the FRCM became ineffective earlier during the fire exposure.
5. Increasing the preloading level (as a percentage of the ultimate capacity of the column) led to a significant reduction in load resistance duration in Series 2 columns. Moreover, higher preloads resulted in less ductile behavior.
6. Series 3A and 3B columns exhibited longer load resistance duration compared to Series 2 columns due to the larger cover and the steel insulation effect.

7. Insulated columns demonstrated substantially longer load resistance due to delayed temperature rise throughout the cross-section. For example, at the FRCM level, column S2_1L_40_ni_B reached 715°C after 65 minutes (leading to failure), while column S4_1L_40_i_B reached around 580°C after 215 minutes before failing.
8. Adding fireproof insulation to Series 4 columns significantly reduced overall displacements compared to uninsulated Series 2 columns. Columns S4_1L_40_i_C and S2_1L_40_ni_C, preloaded to 75% of their ultimate capacity, exhibited axial displacements of 1.6 mm and 3.4 mm, respectively, after approximately 30 minutes of fire exposure.
9. Weakening of the concrete regions closer to the column surface was observed due to their proximity to the fire. Concrete crushing in the core was a common observation at failure in most specimens.
10. FRCM rupture occurred in several Series 2 columns including S1_0L_40_ni_A and S1_0L_40_ni_B, but was not observed in column S1_0L_40_ni_C.
11. Steel yielding was observed in most Series 1 and Series 2 columns. Some columns experienced yielding in longitudinal bars only, while others in both longitudinal and transverse reinforcement.
12. The most common failure mode for FRCM-confined cylinders was separation at the fiber-matrix interface. In a few specimens, rupture or debonding of the FRP strips occurred, leading to premature failure in cylinders 100_2L_30 and 100_1L_45.
13. The effect of the PBO FRCM-confinement was pronounced in cylinders with a concrete strength of 30 MPa, while it was less effective in cylinders with 45 and 70 MPa concrete. These observations were consistent across the heated cylinders as well.
14. Heating the unconfined cylinders to a target temperature of 100°C resulted in a slight increase in strength for all 3 groups of cylinders, likely due to possible prolonged curing of the concrete. Heating the specimens to 400°C generally resulted in marginal differences in strength. However, specimen 800_0L_30 experienced the highest decrease in strength, reaching 82%.
15. Despite the expectation that FRCM-confined specimens would exhibit improved fire resistance compared to FRP-confined specimens (due to the

nature of the binding matrix), both the FE analysis and experimental tests on PBO FRCM-confined cylinders indicated the need for insulation to enhance their fire resistance.

a. Adding FRCM layers to the unstrengthened columns in Series 1 improved the load resistance durations. However, the effectiveness of the FRCM decreased by the time of failure in columns strengthened with 1 and 2 layers of FRCM, suggesting the need of a protective layer.
b. Incorporating a 30 mm layer of fireproof insulation to the columns in Series 4 significantly improved load resistance duration and reduced the column displacements compared to the uninsulated columns in Series 2.
c. Heating the confined cylinders to a target temperature of 800°C resulted in a significant reduction in their capacity compared to their strength at room temperature. This finding further emphasizes the necessity of insulating the externally-bonded composite materials.

References

[1] J. P. Firmo, J. R. Correia, and L. A. Bisby, "Fire behaviour of FRP-strengthened reinforced concrete structural elements: A state-of-the-art review," *Compos B Eng*, vol. 80, pp. 198–216, Jun. 2015, doi: 10.1016/j.compositesb.2015.05.045.

[2] Y. A. Al-Salloum, T. H. Almusallam, H. M. Elsanadedy, and R. A. Iqbal, "Effect of elevated temperature environments on the residual axial capacity of RC columns strengthened with different techniques," *Constr Build Mater*, vol. 115, pp. 345–361, Jul. 2016, doi: 10.1016/j.conbuildmat.2016.04.041.

[3] L. Ombres, "Analysis of the bond between Fabric Reinforced Cementitious Mortar (FRCM) strengthening systems and concrete," *Compos B Eng*, vol. 69, pp. 418–426, 2015, doi: 10.1016/j.compositesb.2014.10.027.

[4] K. Al-Lami, T. D'Antino, and P. Colombi, "Durability of fabric-reinforced cementitious matrix (FRCM) composites: A review," *Applied Sciences (Switzerland)*, vol. 10, no. 5, Mar. 2020, doi: 10.3390/app10051714.

[5] D. Lau, Q. Qiu, A. Zhou, and C. L. Chow, "Long term performance and fire safety aspect of FRP composites used in building structures," *Construction and Building Materials*, vol. 126. Elsevier Ltd, pp. 573–585, Nov. 15, 2016. doi: 10.1016/j.conbuildmat.2016.09.031.

[6] J. Donnini, F. de Caso y Basalo, V. Corinaldesi, G. Lancioni, and A. Nanni, "Fabric-reinforced cementitious matrix behavior at high-temperature: Experimental and numerical results," *Compos B Eng*, vol. 108, pp. 108–121, Jan. 2017, doi: 10.1016/j.compositesb.2016.10.004.

[7] N. Tello, Y. Alhoubi, F. Abed, A. el Refai, and T. El-Maaddawy, "Circular and square columns strengthened with FRCM under concentric load," *Compos Struct*, vol. 255, Jan. 2021, doi: 10.1016/j.compstruct.2020.113000.

[8] Y. Alhoubi, A. el Refai, F. Abed, T. El-Maaddawy, and N. Tello, "Strengthening pre-damaged RC square columns with fabric-reinforced cementitious matrix (FRCM): Experimental investigation," *Compos Struct*, vol. 294, p. 115784, Aug. 2022, doi: 10.1016/j.compstruct.2022.115784.

[9] F. Abed, A. ElRefai, T. El-Maaddawy, N. Tello, and Y. Alhoubi, “Strengthening Square and Circular Low-Strength Concrete Columns with Fiber-Reinforced Cementitious Matrix: Experimental Investigation,” *Practice Periodical on Structural Design and Construction*, vol. 27, no. 2, May 2022, doi: 10.1061/(asce)sc.1943-5576.0000676.

[10] L. Bisby, V. Kodur, and M. Green, “Fire_Endurance_of_Fiber-Reinforced Polymer-Confined”.

[11] M. Kamara, S. Yehia, B. St, and P. Zambrano, “Fire and Concrete Structures Related papers Performance of St ruct ures Exposed t o Ext reme High Temperat ure-An Overview Best Pract ice Guidelines for St ruct ural Fire Resist ance Design of Concret e and St eel Buildings,” 2008.

[12] K. T. Q. Nguyen, S. Navaratnam, P. Mendis, K. Zhang, J. Barnett, and H. Wang, “Fire safety of composites in prefabricated buildings: From fibre reinforced polymer to textile reinforced concrete,” *Compos B Eng*, vol. 187, Apr. 2020, doi: 10.1016/j.compositesb.2020.107815.

[13] American Concrete Institute. and ACI Committee 440., *Guide for the design and construction of externally bonded FRP systems for strengthening concrete structures*. American Concrete Institute, 2017.

[14] L. Ombres, “Structural performances of thermally conditioned PBO FRCM confined concrete cylinders,” *Compos Struct*, vol. 176, pp. 1096–1106, Sep. 2017, doi: 10.1016/j.compstruct.2017.06.026.

[15] G. Cerniauskas, Z. Tetta, D. A. Bournas, and L. A. Bisby, “Concrete confinement with TRM versus FRP jackets at elevated temperatures,” *Materials and Structures/Materiaux et Constructions*, vol. 53, no. 3, Jun. 2020, doi: 10.1617/s11527-020-01492-x.

[16] “Abaqus/CAE User’s Manual Abaqus 6.11 Abaqus/CAE User’s Manual.”

[17] V. Kodur, “Properties of concrete at elevated temperatures,” *ISRN Civil Engineering*, vol. 2014, 2014, doi: 10.1155/2014/468510.

[18] V. K. R. Kodur, L. A. Bisby, and M. F. Green, "Preliminary guidance for the design of FRP-strengthened concrete members exposed to fire," *Journal of Fire Protection Engineering*, vol. 17, no. 1, pp. 5–26, Feb. 2007, doi: 10.1177/1042391507061956.

[19] "Structural performance of FRP composites in Fire".

[20] S. K. Foster, L. A. Bisby, and P. Eng, "Fire Survivability of Externally Bonded FRP Strengthening Systems", doi: 10.1061/ASCE1090-0268200812:5553.

[21] R. A. Hawileh, A. Abu-Obeidah, J. A. Abdalla, and A. Al-Tamimi, "Temperature effect on the mechanical properties of carbon, glass and carbon-glass FRP laminates," *Constr Build Mater*, vol. 75, pp. 342–348, Jan. 2015, doi: 10.1016/j.conbuildmat.2014.11.020.

[22] B. Williams, L. Bisby, V. Kodur, M. Green, and E. Chowdhury, "Fire insulation schemes for FRP-strengthened concrete slabs," *Compos Part A Appl Sci Manuf*, vol. 37, no. 8, pp. 1151–1160, Aug. 2006, doi: 10.1016/j.compositesa.2005.05.028.

[23] "ASTM E119: Standard Test Methods for Fire Tests of Building Construction and Materials." [Online]. Available: www.aslm.org

[24] L. N. Koutas, Z. Tetta, D. A. Bournas, and T. C. Triantafillou, "Strengthening of Concrete Structures with Textile Reinforced Mortars: State-of-the-Art Review," *Journal of Composites for Construction*, vol. 23, no. 1, p. 03118001, Feb. 2019, doi: 10.1061/(asce)cc.1943-5614.0000882.

[25] S. M. Raoof and D. A. Bournas, "Bond between TRM versus FRP composites and concrete at high temperatures," *Compos B Eng*, vol. 127, pp. 150–165, Oct. 2017, doi: 10.1016/j.compositesb.2017.05.064.

[26] H. Asgharigharakheili, "Investigation of Tensile Strength of Carbon Fabric-Reinforced Cementitious Matrix (FRCM) at High Temperatures."

[27] E. U. Chowdhury, L. A. Bisby, M. F. Green, and V. K. R. Kodur, "Investigation of insulated FRP-wrapped reinforced concrete columns in fire," *Fire Saf J*, vol. 42, no. 6–7, pp. 452–460, Sep. 2007, doi: 10.1016/j.firesaf.2006.10.007.

[28] T. Trapko, "The effect of high temperature on the performance of CFRP and FRCM confined concrete elements," *Compos B Eng*, vol. 54, no. 1, pp. 138–145, 2013, doi: 10.1016/j.compositesb.2013.05.016.

[29] K. H. Tan and Y. Zhou, "Performance of FRP-Strengthened Beams Subjected to Elevated Temperatures," *Journal of Composites for Construction*, vol. 15, no. 3, pp. 304–311, Jun. 2011, doi: 10.1061/(asce)cc.1943-5614.0000154.

[30] P. P. Bhatt, V. K. R. Kodur, A. M. Shakya, and T. Alkhrdaji, "Performance of insulated FRP-strengthened concrete flexural members under fire conditions," *Frontiers of Structural and Civil Engineering*, vol. 15, no. 1, pp. 177–193, Feb. 2021, doi: 10.1007/s11709-021-0714-z.

[31] Z. Ding *et al.*, "Strengthening concrete using phosphate cement-based fiber-reinforced inorganic composites for improved fire resistance," *Constr Build Mater*, vol. 212, pp. 755–764, Jul. 2019, doi: 10.1016/j.conbuildmat.2019.04.038.

[32] S. M. Raoof and D. A. Bournas, "TRM versus FRP in flexural strengthening of RC beams: Behaviour at high temperatures," *Constr Build Mater*, vol. 154, pp. 424–437, Nov. 2017, doi: 10.1016/j.conbuildmat.2017.07.195.

[33] Z. C. Tetta and D. A. Bournas, "TRM vs FRP jacketing in shear strengthening of concrete members subjected to high temperatures," *Compos B Eng*, vol. 106, pp. 190–205, Dec. 2016, doi: 10.1016/j.compositesb.2016.09.026.

[34] M. Kyaure and F. Abed, "Finite element parametric analysis of RC columns strengthened with FRCM," *Compos Struct*, vol. 275, Nov. 2021, doi: 10.1016/j.compstruct.2021.114498.

[35] O. El-Mahdy, G. Hamdy, and M. Hisham, "NONLINEAR FINITE ELEMENT ANALYSIS OF INSULATED FRP STRENGTHENED REINFORCED CONCRETE COLUMNS SUBJECTED TO FIRE," *Stavební obzor - Civil Engineering Journal*, vol. 27, no. 2, pp. 195–210, 2018, doi: 10.14311/cej.2018.02.0016.

[36] J.-G. Dai, W.-Y. Gao, and J. G. Teng, "Finite Element Modeling of Insulated FRP-Strengthened RC Beams Exposed to Fire," *Journal of Composites for*

Construction, vol. 19, no. 2, p. 04014046, Apr. 2015, doi: 10.1061/(asce)cc.1943-5614.0000509.

[37] S. Mirzabagheri and O. (Sam) Salem, "Parametric study on the residual compressive strength of RC columns subjected to different standard fire durations and load ratios," *Journal of Structural Fire Engineering*, 2022, doi: 10.1108/JSFE-04-2022-0017.

[38] A. Nair and O. (Sam) Salem, "Experimental determination of the residual compressive strength of concrete columns subjected to different fire durations and load ratios," *Journal of Structural Fire Engineering*, vol. 11, no. 4, pp. 529–543, Oct. 2020, doi: 10.1108/JSFE-10-2019-0034.

[39] S. Sayyar Roudari, T. M. Abu-Lebdeh, and S. Sayyar Roudsari, "Evaluation of Fire Effects on Reinforced Concrete Columns Using Finite Element Method Evaluation of Fire Effects on Reinforced Concrete Columns Using Finite Element Method Evaluation of Fire Effects on Reinforced Concrete Columns Using Finite Element Method," *American Journal of Engineering and Applied Sciences Original Research Paper*, 2019, doi: 10.3844/ajeassp.2019.227.235ï.

[40] M. Mohamed Bikhiet, N. F. El-Shafey, and H. M. El-Hashimy, "Behavior of reinforced concrete short columns exposed to fire," *Alexandria Engineering Journal*, vol. 53, no. 3, pp. 643–653, 2014, doi: 10.1016/j.aej.2014.03.011.

[41] "EN 1992-1-2: Eurocode 2: Design of concrete structures - Part 1-2: General rules - Structural fire design," 1992.

[42] "EN 1993-1-2: Eurocode 3: Design of steel structures - Part 1-2: General rules - Structural fire design," 1993.

[43] R. Černý, J. Toman, J. Poděbradská, and P. Rovnaníková, "Thermal Properties of Building Materials in High Temperature Range."

[44] M. F. Anuar, P. Shafigh, A. Ma'amor, S. Yousuf, and F. W. Akashah, "Experimental analysis of changes in cement mortar containing oil palm boiler clinker waste at elevated temperatures in different cooling conditions," *Crystals (Basel)*, vol. 11, no. 8, Aug. 2021, doi: 10.3390/cryst11080988.

[45] R. B. George, S. E. Thomas, and A. Professor, "Analytical Study of FRCM under Elevated Temperature," *International Journal of Scientific Engineering and Research (IJSER) www.ijser.in ISSN*, vol. 4, pp. 2347–3878, 2015, [Online]. Available: www.ijser.in

[46] F. ACI Committee 549, "Guide to design and construction of externally bonded fabric-reinforced cementitious matrix and steel-reinforced grout systems for repair and strengthenng of concrete structures."

[47] F. Abed, C. Oucif, Y. Awera, H. H. Mhanna, and H. Alkhraisha, "FE modeling of concrete beams and columns reinforced with FRP composites," *Defence Technology*, vol. 17, no. 1, pp. 1–14, Feb. 2021, doi: 10.1016/j.dt.2020.02.015.

[48] V. K. R. Kodur, L. A. Bisby, and M. F. Green, "Experimental evaluation of the fire behaviour of insulated fibre-reinforced-polymer-strengthened reinforced concrete columns," *Fire Saf J*, vol. 41, no. 7, pp. 547–557, Oct. 2006, doi: 10.1016/j.firesaf.2006.05.004.

[49] ANSYS Inc., "ANSYS–Release Version 12.1.0." 2009.

[50] "MapeWrap C Uni-Ax 600, technical sheet | Mapei." https://www.mapei.com/pr/en-us/products-and-solutions/products/detail/mapewrap-c-uni-ax-600 (accessed Aug. 28, 2022).

[51] "Standard Test Method for Compressive Strength of Cylindrical Concrete Specimens 1."

[52] D. Anupama Krishna, R. S. Priyadarsini, and S. Narayanan, "Effect of elevated temperatures on the mechanical properties of concrete," in *Procedia Structural Integrity*, Elsevier B.V., 2019, pp. 384–394. doi: 10.1016/j.prostr.2019.05.047.

[53] M. Ghandehari, ; Ali Behnood, and M. Khanzadi, "Residual Mechanical Properties of High-Strength Concretes after Exposure to Elevated Temperatures", doi: 10.1061/ASCE0899-1561201022:159.

[54] A. M. Zeyad *et al.*, "Review on effect of steam curing on behavior of concrete," *Cleaner Materials*, vol. 3. Elsevier Ltd, Mar. 01, 2022. doi: 10.1016/j.clema.2022.100042.

[55] S. Y. N. Chan, G.-F. Peng, and J. K. W. Chan, “Comparison between high strength concrete and normal strength concrete subjected to high temperature,” 1996.

Vita

Reem Talo was born in 1996, in Michigan, United States. She received her primary education in Damascus, Syria and secondary education in Abu Dhabi, UAE. She received her B.Sc. degree in Civil Engineering from Abu Dhabi University in 2019.

In September 2020, she joined the Civil Engineering master's program in the American University of Sharjah as a graduate research and teaching assistant. During her master's study, she co-authored several papers which were presented in international conferences. Her area of research includes studying the behaviour of concrete structures exposed to fire and concrete strengthening; particularly, column strengthening.